Dynamic reorganization and selective segregation of mitochondria under DarT-mediated mtDNA damage

Nitish Dua, Akshaya Seshadri and Anjana Badrinarayanan*

National Centre for Biological Sciences - Tata Institute of Fundamental Research, Bellary Road, Bangalore 560065, Karnataka, India, Phone: 91 80 23666547

*Correspondence to: anjana@ncbs.res.in

Keywords

S. cerevisiae, mtDNA, DNA damage, mitochondrial fission and fusion, DarT, single-cell imaging, fluorescence microscopy

Abstract:

Mitochondria are dynamic organelles that play essential roles in cell growth and survival. Processes of fission and fusion are critical for distribution, segregation and maintenance of mitochondria and their genomes (mtDNA). While recent work has revealed the significance of mitochondrial organization for mtDNA maintenance, impact of mtDNA perturbations on mitochondrial dynamics remains less understood. Here we develop a tool to induce mitochondria-specific DNA damage, using a mitochondrial-targeted base modifying bacterial toxin, DarT. Following damage, we observe dynamic reorganization of mitochondrial networks, likely driven by mitochondrial dysfunction. Changes in organization are associated with loss of mtDNA, independent of mitophagy. Unexpectedly, perturbation to exonuclease function of mtDNA replicative polymerase, Mip1, results in rapid loss of mtDNA. Our data suggest that, under damage, partitioning of defective mtDNA and organelle are de-coupled, with emphasis on mitochondrial segregation independent of its DNA. Together, our works underscores the importance of genome maintenance on mitochondrial function, that can act as a modulator of organelle organization and segregation.

41 **Introduction:**

42 Mitochondrial networks are highly dynamic and undergo changes in shape and size
43 throughout the cell cycle (Westermann, 2010). These dynamics are predominantly attributed
44 to two processes of fission and fusion, carried out by evolutionarily conserved machineries
45 (Westermann, 2008). In budding yeast, fission of mitochondria is carried out by Dnm1, which
46 is recruited to the outer membrane by adaptor proteins. Fusion of mitochondria occurs at the
47 level of the inner membrane (carried out by Mgm1) as well as the outer membrane, via Fzo1
48 (Scott & Youle, 2010; Shaw & Nunnari, 2002). Fission and fusion are required for proper
49 distribution and segregation of mitochondria during cell division and also essential for
50 moulding the organelle network in response to changing growth conditions (Detmer & Chan,
51 2007). Along with facilitating dynamic adaptation of mitochondrial function to the metabolic
52 needs of the cell (Bagamery et al., 2020; Laporte et al., 2018), they play a crucial role in quality
53 control of the organelle (Detmer & Chan, 2007; Ni et al., 2015).

54 Apart from ensuring organelle health, fission and fusion are also important for maintaining
55 mitochondrial genome integrity and its DNA copy numbers (Busch et al., 2014; Lewis et al.,
56 2016; Lieber et al., 2019; Osman et al., 2015). All eukaryotic cells, with a few exceptions,
57 contain multiple copies of mtDNA (chiefly encoding for part of the electron transport chain
58 as well as mitochondrial translation RNAs and proteins) and are distributed throughout the
59 organelle network (Brown et al., 2011; Chen & Butow, 2005; Osman et al., 2015). These DNA
60 copies are packaged in the form of nucleoids (Farge et al., 2012), primarily by Abf2 in budding
61 yeast (Chen & Butow, 2005). Studies have shown that mtDNA nucleoids are non-randomly
62 distributed in the mitochondrial network, and are present equidistant from each other
63 (Osman et al., 2015). This organization appears to be essential for ensuring segregation of
64 accurate amounts of mtDNA during cell division (Jajoo et al., 2016). Indeed, lowered levels of
65 mtDNA replication are observed when mitochondrial fusion is perturbed, leading to a
66 decrease in mtDNA copy numbers (Ramos et al., 2019). Mitochondrial fission is also linked to
67 mtDNA replication and segregation in budding yeast and facilitates distribution of mtDNA
68 throughout the mitochondrial network (Lewis et al., 2016). Previous studies have also
69 reported that deletions on mtDNA occur when pathways of fission and fusion are perturbed
70 (Osman et al., 2015).

71 Accurate maintenance of mtDNA integrity is critical, as mutations on mtDNA can have adverse
72 effects on cell survival and are associated with several human pathologies (Hahn & Zuryn,

2019; Scheibye-Knudsen et al., 2015; Taylor & Turnbull, 2005). Close proximity of mtDNA to the electron transport chain makes it susceptible to damage via reactive species generated during oxidative phosphorylation (Alexeyev et al., 2013; Yakes & Van Houten, 1997). Even under physiological conditions, mtDNA accumulates mutations and deletions over time; these are also proposed to be major drivers of ageing (Alexeyev et al., 2013; Richter, 1995; Wallace, 2010).

How do cells respond to mtDNA damage? There is evidence for the localization of certain DNA repair proteins to the mitochondria (such as those involved in base excision repair and recombination) (Alexeyev et al., 2013; Boesch et al., 2011; Scheibye-Knudsen et al., 2015; Stevnsner et al., 2002). However, certain repair pathways seem to be absent from the mitochondria (for example, nucleotide excision repair) (Clayton et al., 1974; Pascucci et al., 1997). Thus, while DNA repair pathways have been detected in the mitochondria, importance and regulation of mtDNA damage repair has remained unclear. Since mtDNA can directly affect functionality of the organelle, it is possible that one layer of quality control is carried out by mechanisms that respond to mitochondrial dysfunction directly. Indeed, in response to organelle dysfunction, cells employ fission and fusion machineries to clear out any damaged mitochondria (Ni et al., 2015). For example, regulation of fusion can facilitate complementation of mutations present on mitochondrial genomes (Nakada et al., 2001). Similarly, mitochondrial fission helps in selective removal and degradation of mitochondria via PINK-Parkin mediated mitophagy or even mitocytosis (Jiao et al., 2021; Jin & Youle, 2012; Zhang et al., 2019). More recently, a role for mitochondrial reorganization at the level of the cristae has also been discovered to contribute to segregation of defective mitochondrial domains, arising from mutant mtDNA copies (Jakubke et al., 2021). It is likely that these pathways contribute to different degrees of quality control, depending on the cell type and specific growth environments (Pickles et al., 2018). Although it is becoming increasingly evident that mitochondrial dynamics can regulate mtDNA synthesis, partitioning and homeostasis, the influence of mtDNA damage on mitochondrial organization and segregation is not fully understood. A major challenge in studying mtDNA damage response and repair has been the ability to generate mtDNA-specific damage. In this context, tools to make mtDNA-specific DSBs have been invaluable, but are dependent on the presence of specific sequences on the mtDNA to allow for targeted action of the enzyme. In most cases, generic

damaging agents that can cause adducts or lesions on DNA (nuclear and mitochondrial) preclude the ability to disentangle mitochondria-specific effects.

To characterize the impact of mtDNA perturbations on organelle organization and function, we developed a novel system to generate inducible mtDNA-specific damage in *S. cerevisiae*. We engineered a mitochondrially-targeted bacterial toxin, mtDarT (which generates adducts on single-stranded DNA) (Jankevicius et al., 2016) to probe the effect of mtDNA damage on mitochondrial dynamics in real-time. We find that mtDNA damage drives network fragmentation; based on our observations, we suggest that this is likely due to a lowering in fusion rates arising from mitochondrial dysfunction. We further implicate a critical role for the exonuclease function of the mtDNA polymerase in mtDNA maintenance under damage. Our study reveals an intricate connection between mtDNA integrity, mitochondrial function and its role in regulating organelle organization and segregation.

117 **Results:**

118 **System to induce mitochondria-specific DNA damage**

119 To perturb mtDNA integrity and observe the resultant mitochondrial dynamics in real-time,
120 we developed an mtDNA-specific damage inducing system in *S. cerevisiae*. For this, we utilized
121 a bacterial toxin, DarT, that is part of a widely conserved DarT-DarG toxin-antitoxin system
122 (Jankevicius et al., 2016). DarT functions via transferring an ADP-ribosyl group on single-
123 stranded DNA using NAD+ as a substrate (Fig. 1A) and has been shown to generate DNA
124 damage-inducing adducts on the bacterial genome (likely via blocking replication progression)
125 (Lawarée et al., 2020). The adduct is attached to a thymidine within a 'TNTC' motif
126 (Jankevicius et al., 2016; Schuller et al., 2021)., which is present abundantly on the
127 mitochondrial genome.

128 We constructed a mitochondrial matrix-targeted DarT (derived from *T. aquaticus*), mtDarT,
129 via fusion of DarT to the first 69 amino acids of SU9 (subunit 9 of the F_1-F_0 ATPase) (Horie et
130 al., 2003). A 3XFlag-tag was added to the C-terminus of DarT, to enable verification of
131 expression as well as localization upon induction (Fig. S1A). mtDarT was expressed from a β-
132 estradiol inducible-promoter on a low copy plasmid (Louvion et al., 1993). This strategy was
133 employed to separately express a catalytically dead variant of DarT (DarTE160A), which
134 retains only negligible DarT activity (Jankevicius et al., 2016). We first confirmed expression
135 of mtDarT, as well as mtDarTE160A via western blotting after 4 and 8hr of induction with
136 100nM β-estradiol (Fig. S1B). Immunostaining using an anti-flag antibody revealed that the
137 proteins indeed localized to the mitochondria, marked using mitochondrially-targeted
138 mNeonGreen (mt-mNG) (Fig. 1B, S1C).

139 We next assessed the impact of mtDarT on cell growth, utilizing the ability of yeast cells to
140 show differential growth on fermentable/ non-fermentable carbon sources, based on their
141 mitochondrial activity (Ephrussi et al., 1955). Cells with impaired mitochondrial function are
142 able to survive on media containing a fermentable carbon source (albeit forming smaller,
143 'petite' colonies), due the ability of these cells to carry out glycolysis. However, such cells are
144 compromised for growth on non-fermentable carbon sources, where oxidative
145 phosphorylation (and hence complete mitochondrial function) is essential. When compared
146 with an empty vector control, we found that cells expressing mtDarT showed no associated

147 loss in viability on plates supplemented with dextrose (fermentable carbon source) (Fig. 1C).
148 These cells showed significant loss of viability in case of plates supplemented with glycerol
149 (non-fermentable carbon source) (Fig. 1C). Importantly, the growth defects observed were
150 mtDarT-specific and required the DNA adduct-forming catalytic function of DarT (Fig. 1C).

151 To further establish mitochondria-specific mtDarT effects, we carried out a dot-blot assay, to
152 probe for ADPr groups on both nuclear and mitochondrial DNA. We observed signal only for
153 mtDNA, dependent on mtDarT expression (Fig.1D). In addition, we assessed the localization
154 of Lcd1p (or Ddc2p), that is reported to localize to the nucleus under nuclear DNA damage or
155 replication stress ((Lisby et al., 2004; Melo et al., 2001); Fig. S1D, HU-treated cells). Upon
156 mtDarT induction, we did not observe an increase in the number of cells with Lcd1p
157 localizations (Fig. S1D). Together, these results supported the idea that mtDarT had
158 mitochondria-specific action.

159 **mtDNA damage impacts mitochondrial organization and dynamics**

160 We next characterized the impact of mtDNA damage on mitochondrial organization and
161 function in glycolysis replete conditions. For this, we followed mitochondrial dynamics in cells
162 expressing Cox4-mCherry to track mitochondria in addition to mtDarT (or an empty vector
163 control). We classified the observed mitochondrial organizations into three distinct
164 categories: 'tubular', 'fragmented' and 'aggregate' (representative examples are shown in Fig.
165 2A). We found that the induction of mtDarT resulted in fragmentation of the mitochondrial
166 network (Fig. 2A-B), with an increase in percentage of cells with fragmented or aggregate
167 mitochondria. Indeed, cells carrying mtDarT displayed some perturbation to mitochondrial
168 organization even prior to induction, likely due to leaky expression from the vector (Fig. S2A).

169 We next followed the mtDarT-induced changes in mitochondrial organization over time via
170 measuring two features (Fig. 2C): a. the mean form factor (MFF) of mitochondria per cell, an
171 indicator of mitochondrial circularity (Chaudhry et al., 2020) and b. the number of discrete
172 mitochondria per cell. We plotted MFF and number of mitochondria for all cells as 2D density
173 plots, allowing us to visualize populations of cells having either tubular, fragmented or
174 aggregated mitochondria (Fig. 2C). We observed that control cells harboring an empty vector
175 largely populated MFF above 2 (predominantly tubular mitochondrial morphology) and

176 maximum density represented an intermediate between a tubular network and fragmented
177 state (Fig. 2D). This is as expected under unperturbed conditions, given the dynamic nature
178 of the mitochondria throughout the cell cycle (Shaw & Nunnari, 2002). In contrast, upon
179 mtDarT induction, mitochondria gradually transitioned from tubular (MFF >2) to fragmented/
180 aggregate states, having MFF <2 (Fig. 2D).

181 Organization of the mitochondrial network is regulated by a dedicated set of GTPases that
182 control mitochondrial membrane fission and fusion (Westermann, 2008). Hence, to assess
183 the contribution of changes in mitochondrial fission and/ or fusion upon mtDNA damage, we
184 followed mitochondrial dynamics via time-lapse microscopy. We imaged cells at 5 min
185 intervals for 40 min, after 4hr of damage exposure (Fig. 2E, S2B-C) and plotted density plots
186 as described above. Transition from tubular to fragmented states would reveal fission events,
187 while transition in the opposite direction (towards a tubular network) would be indicative of
188 fusion events.

189 To assess the impact of mtDNA damage on fission dynamics, we followed cells (control and
190 damage) with tubular mitochondrial networks at the start of imaging (T0), after pre-induction.
191 We found that the rates of mitochondrial fission (as assessed by transition of cells with MFF
192 >2 to MFF <2), were comparable between control and damage-treated cells (Fig. S2D). In line
193 with this observation, we did not find an increase in levels of the fission protein Dnm1
194 (Bleazard et al., 1999) (Fig. S2E). Another mechanism for mitochondrial fission, independent
195 of changes in the levels of Dnm1, is via ERMES contact sites (Lewis et al., 2016). An increase
196 in the number of these contact sites (which can be imaged via tracking the number of Mdm34
197 localizations) could lead to recruitment of Dnm1, thereby resulting in an increase in fission
198 events. However, we did not observe a significant increase in the number of ERMES contact
199 sites in cells facing damage (Fig. S2F).

200 Unlike the observed fission dynamics, cells facing mtDarT-induced damage had significantly
201 lower fusion events. When we followed individual cells over time, we found that mtDarT-
202 expressing cells with fragmented or aggregate mitochondrial organization did not display
203 dynamic reorganization towards a network morphology (Fig. 2E, S2C). Consistently, in
204 comparison to the control, cells expressing mtDarT were compromised in transitioning from
205 MFF <2 to MFF >2 (fragmented to tubular transition) and tended to maintain the density

206 distribution observed at the start of the experiment (Fig. 2F). The control cells on the other
207 hand were able to dynamically transition from MFF <2 to MFF>2 within the 40 min imaging
208 interval (Fig.2E-F). Importantly, the above described effects of mtDarT were not cell size or
209 cell cycle-stage specific (as assessed by the presence and size of the bud), further
210 underscoring the direct impact of mtDNA damage on mitochondrial organization (Fig. S3A-
211 B).Taken together, our data suggest that mtDNA damage drives a large scale reorganization
212 of the mitochondrial network, likely via an impact on mitochondrial fusion rates. Indeed,
213 although we did not observe a significant change in the levels of fusion protein, Fzo1p (Fig.
214 S2E, S2G), it is possible that other mechanisms contribute to the observed mitochondrial
215 dynamics under damage (see Discussion).

216 **mtDNA damage results in mitochondrial dysfunction**

217 Given our observations on the impact of mtDNA damage on mitochondrial membrane fusion
218 dynamics, we wondered whether mitochondrial function was perturbed in these cells. We
219 thus measured two indicators of mitochondrial activity: a. mitochondrial membrane potential
220 (ψ) via imaging TMRE (a membrane potential sensitive dye) and b. oxygen consumption rate
221 (OCR) using a Seahorse assay (Ludovico et al., 2001). We observed a decrease in membrane
222 potential in cells expressing mtDarT (Fig. 3A), similar to impact of FCCP, a membrane
223 decoupler which decreases ψ (Fig. S4A). Similarly, mtDarT-treated cells also had lower OCR
224 (Fig. S4B). Together, these observations suggest that mitochondrial function in mtDarT-
225 treated cells is compromised (we use the term 'dysfunction' to encompass both these
226 parameters of mitochondrial function). Importantly, lowering in membrane potential was
227 observed even in mtDarT cells with reticular/ tubular networks, suggesting that mitochondrial
228 dysfunction upon mtDNA damage preceded changes in mitochondrial organization and
229 dynamics (Fig. S4D).

230 Specific lowering in mitochondrial fusion rates has been reported in cells with compromised
231 membrane potential (and hence dysfunction) (Duvezin-Caubet et al., 2006; Karbowski et al.,
232 2004; Legros et al., 2004; Twig et al., 2008). We thus hypothesized that mtDNA damage-
233 induced mitochondria with lowered membrane potential would display lower probability of
234 fusion, when compared with mitochondria with unperturbed membrane potential. To assess
235 this, we tracked mitochondrial dynamics (via mt-mNeongreen) in mtDarT-treated cells after

236 a brief pulse of TMRE staining (Fig. 3B-C). We then analysed the mean form factor and number
237 of mitochondria for cells specifically having MFF<2 (fragmented) along with their initial TMRE
238 fluorescence intensities, and asked whether these mitochondria were able to transition to a
239 tubular state. We observed that mitochondria with higher membrane potential, but
240 aggregate/ fragmented organization (MFF <2) were able to fuse into tubular mitochondrial
241 networks (MFF >2) (Fig. 3C-D). In contrast, fragmented mitochondria with lower membrane
242 potential were unable to do so during the course of imaging (Fig. 3C-D).

243 Our observations are consistent with the possibility that mtDNA damage results in
244 mitochondrial dysfunction (reduced membrane potential and compromised OCR), which in-
245 turn affects mitochondrial dynamics via impairing fusion.

246 **Changes in mitochondrial morphology accompany loss of mtDNA but not mitochondria**

247 We next assessed the effects of mtDarT damage on mtDNA, and whether the observed
248 mitochondrial dynamics contributed to clearance of damaged DNA/ dysfunctional
249 mitochondria. Following a previously-described method, we stained cells with SYBR Green I
250 to visualize mtDNA nucleoids (Jajoo et al., 2016) (Fig. 4A). In the control sample without
251 mtDNA damage, less than 2% cells had no detectable mtDNA foci ('ρ0' cells) at all time points
252 of imaging (Fig. 4B). In contrast, upon mtDarT induction, the percentage of ρ0 cells steadily
253 increased, with ~30% cells having no detectable foci post 8hr of damage induction (Fig. 4B).
254 Consistent with this, we also observed an overall decrease in the number of mtDNA foci per
255 cell upon mtDNA damage (Fig. S5A).

256 In some instance mitochondrial dysfunction (and associated fragmentation) has been shown
257 to occur in conjunction with mitophagy (Burman et al., 2017; Kleele et al., 2021). We thus
258 asked whether loss of mtDNA under damage was a result of clearance of dysfunctional
259 mitochondria. For this, we assessed the levels of two nuclear-encoded mitochondrial
260 proteins, Cox4 and Tom20, via western blot. We found that levels of these proteins did not
261 change significantly under damage conditions (Fig. 4C). This is in contrast to mitochondrially-
262 encoded Cox2p levels, that decreases upon mtDarT expression (Fig. S4C). We then measured
263 mitochondrial volume (Harwig et al., 2018) (Fig. S5B) and found that here too, no significant
264 changes were observed over time. Consistent with the lack of change in mitochondrial
265 content, we did not observe an increase in mitophagy-associated marker, Atg8 (Torggler et

266 al., 2017) localizations (Fig. S5C), or a significant increase in the number of Atg8 localizations
267 associated with mitochondria (Böckler & Westermann, 2014) (Fig. S5D). We also did not
268 detect a significant difference in the amount of vacuolar localization of Idh1 (Kanki & Klionsky,
269 2008) upon mtDarT-induction (Fig. S5E). This suggested that an mtDNA-specific mechanism
270 might be responsible for mtDNA clearance in response to damage.

271 **Exonuclease activity of the mtDNA polymerase, Mip1, is essential for mtDNA maintenance**

272 In mammalian cells, the mtDNA replicative polymerase PolG can switch between synthesis
273 and degradation functions to clear out defective mtDNA (Nissanka et al., 2018; Peeva et al.,
274 2018). Evidence for such exonuclease function of the yeast homolog, Mip1, has also been
275 reported in conditions of starvation or oxidative stress (Medeiros et al., 2018). We hence
276 asked whether exonuclease activity could contribute to mtDNA clearance under mtDarT-
277 induced damage. For this, we blocked the exonuclease activity of Mip1, via mutating the
278 catalytic site (D171A, E173A) responsible for its degradative function (Foury &
279 Vanderstraeten, 1992; Medeiros et al., 2018) (Fig. 5A) and assessed presence of mtDNA
280 nucleoids via SYBR Green I staining. Surprisingly, upon mtDarT induction, we observed that
281 Mip1 exonuclease deficient cells generated ρ0 cells significantly faster than wild type. As
282 shown earlier (Fig. 4B), 30% of wild type cells were ρ0 after 8hr of mtDarT induction. *mip1*$^{exo-}$
283 cells already generated ρ0 cells at a low frequency (~7%) in no damage conditions,
284 highlighting that inability to clear damaged mtDNA (in this case likely due to replication
285 errors) results in mtDNA loss in glucose replete growth environment. In line with this
286 observation, induction of mtDNA damage resulted in 60% cells becoming ρ0 post 8 hr of
287 mtDarT induction (Fig. 5B). Importantly, rapid mtDNA loss did not result in production of cells
288 devoid of mitochondria.

289 How do *mip1*$^{exo-}$ cells lose mtDNA in such a rapid manner under damage? We measured
290 budding events of wild type and mutant cells upon mtDNA damage and found them to be
291 comparable during the course of the experiment (3±1 budding events over 6 hr, for both wild
292 type and *mip1*$^{exo-}$ cells expressing mtDarT), ruling out the possibility of faster division rates in
293 the exonuclease mutant contributing to mtDNA loss over time. We next assessed
294 mitochondrial dynamics in the mutant. As seen in wild type cells, we found that mtDNA
295 damage resulted in significant changes to mitochondrial organization in case of exonuclease
296 deficient cells as well (Fig. S6A). Furthermore, in comparison to mtDarT-treated wild type

297 cells, we found that membrane potential was severely compromised in the mutant (Fig. S6B),
298 suggesting that these cells likely have significantly lowered mitochondrial membrane fusion
299 events. A potential outcome of enhanced mitochondrial dysfunction is a defect in the
300 segregation of mitochondria during division (McFaline-Figueroa et al., 2011). We thus
301 wondered whether this could impact partitioning of the mtDarT-induced damaged mtDNA.
302 Such partitioning defect would likely be more severe/ pronounced in the *mip1*$^{exo-}$ condition,
303 where defective mtDNA would accumulate due to lack of a clearance mechanism.

304 When we probed for mtDNA in these cells, we observed a significant proportion of cells with
305 mitochondria devoid of mtDNA in *mip1*$^{exo-}$ background (Fig 5C). We asked whether mtDNA
306 was differentially partitioned in these cells, resulting in generation of mitochondria devoid of
307 DNA as well. For this, we analysed mother-bud pairs after SYBR Green I staining, and
308 quantified the fraction of mtDNA foci in the bud (Fig. 5D). Consistent with previous reports
309 (Jajoo et al., 2016; Osman et al., 2015), we found that the amount of mtDNA partitioned in
310 the bud scaled with increasing bud area in control as well as wild type cells after mtDarT
311 induction (Fig. 5E). However, unlike wild type cells, there was significant heterogeneity in the
312 amount of mtDNA in the bud (across cell areas) in case of exonuclease deficient cells treated
313 with mtDarT, suggesting imprecise mtDNA partitioning (Fig. 5E), with several instances of
314 buds receiving no mtDNA (ρ0 daughter cells) (Fig. 5E). We hence hypothesized that if such
315 asymmetry indeed contributed to the rapid production of ρ0 cells in the exonuclease deficient
316 mutant, cells arrested for cell cycle progression would no longer generate ρ0 cells at the high
317 frequency observed in case of steady state growth conditions. To assess this, we used *bar1*Δ
318 strains treated with α-factor, that should arrest cells in G1-S transition (Breeden, 1997). We
319 confirmed the same using flow cytometry, as well as via assessing the morphology of the cells
320 upon arrest (Fig. 5F (left) and (Rosebrock, 2017)). In wild type cells, we observed that loss of
321 mtDNA occurred at comparable frequency in arrest and non-arrest conditions. In contrast, in
322 *mip1*$^{exo-}$ background, mtDNA loss was significantly lower under arrest (Fig. 5F (right)). Thus,
323 asymmetric mitochondrial partitioning during cell division could significantly contribute to the
324 rapid production of ρ0 cells in the exonuclease deficient mutant. Taking these observations
325 together, our results suggest that mitochondrial dynamics could differentially impact
326 damaged mtDNA segregation in conditions where defective mtDNA clearance mechanisms
327 are compromised, likely facilitating organelle segregation independent of its DNA.

328 **Discussion:**

329 In this study, we describe a system to generate mtDNA-specific damage in *S. cerevisiae*. Using
330 a bacterial toxin DarT (Jankevicius et al., 2016), targeted to the mitochondria, we follow the
331 impact of mtDNA damage on mitochondrial organization, segregation and function. We find
332 that mtDNA damage affects mitochondrial function via compromising membrane potential.
333 This could be the causative force in mitochondrial reorganization by reduction in
334 mitochondrial membrane fusion events (Duvezin-Caubet et al., 2006; Karbowski et al., 2004;
335 Legros et al., 2004; Twig et al., 2008), facilitating selective segregation of mitochondria
336 without defective mtDNA (discussed below).
337 How cells sense and respond to mtDNA damage remains an outstanding and exciting
338 question. Previous studies have detected the presence of specific DNA repair enzymes
339 (include BER and recombination machinery) in the mitochondria (Alexeyev et al., 2013;
340 Boesch et al., 2011; Scheibye-Knudsen et al., 2015; Stevnsner et al., 2002). While some of
341 these pathways encode mitochondrially-targeted isoforms (Swartzlander et al., 2010), many
342 do not carry any known localization signal (Stuart et al., 2005; Thyagarajan et al., 1996). How
343 they localize to the mitochondria remains unclear, as is the importance of specific repair
344 pathways in mtDNA maintenance (Alexeyev et al., 2013; Scheibye-Knudsen et al., 2015).
345 Indeed, there are certain types of damages (such as UV-induced pyrimidine dimers) for which
346 active repair pathways have not been found in mitochondria (Clayton et al., 1974; Pascucci et
347 al., 1997). In such scenarios, where mtDNA damage becomes persistent, degradation of
348 damaged mtDNA copies has been proposed to occur (Alexeyev et al., 2013; Shokolenko et al.,
349 2013). Interestingly, this function is carried out by the exonuclease activity of the mtDNA
350 polymerase (Mip1 or PolG) itself (Nissanka et al., 2018; Peeva et al., 2018).
351 Our work further underscores a central role for defective mtDNA clearance via exonuclease
352 activity of the replicative polymerase under damage. We propose that Mip1 exonuclease
353 function is required for mtDNA degradation under damage and inability of cells to clear such
354 damaged mtDNA results in rapid generation of ρ0 cells in glucose replete conditions. Although
355 in unperturbed conditions, mtDNA and mitochondrial segregation may be coordinated (Jajoo
356 et al., 2016; Lewis et al., 2016; Osman et al., 2015), our observations support a role for
357 selective segregation of damaged mtDNA, in a manner that can result in partitioning of
358 mtDNA-less mitochondria in the daughter cells. Generation of cells devoid of mtDNA, without

359 significant loss of mitochondria would suggest cells can de-couple mtDNA and mitochondrial
360 partitioning and maintenance under conditions of damage, when complete mitochondrial
361 function may not be essential (such as in glycolytic conditions). Indeed, while mitochondria
362 cannot be made *de novo* (Westermann, 2014), ρ0 and ρ- cells in the environment could regain
363 and complement lost mtDNA, albeit with different proficiencies (Ling et al., 2019; Perlman,
364 1976).
365 It is interesting to note that mtDNA damage triggers rapid changes in mitochondrial
366 organization and segregation, both outcomes potentially stemming from mitochondrial
367 dysfunction. It would be important to understand how mtDNA damage causes perturbations
368 to mitochondrial function and how this in turn modulates rates of fusion. Although levels of
369 Fzo1 did not change under mtDNA damage, it would be informative to understand what other
370 mechanisms might regulate mitochondrial fusion to result in the observed dynamics in
371 budding yeast. For example, mtDNA damage can perturb levels of mitochondrially-encoded
372 proteins such as those part of the electron transport chain (Fig. S4C), which requires
373 coordinated effort from nuclear and mitochondrial genomes (Fontanesi et al., 2006;
374 Herrmann & Funes, 2005). This can adversely affect maintenance of mitochondrial membrane
375 potential. Separately, studies have reported a direct impact of lowered membrane potential
376 on differential processing of Opa1 (a mitochondrial membrane fusion protein in mammals),
377 affecting its association with the mitochondrial membrane (Song et al., 2007).
378
379 The change in mitochondrial organization we report is consistent with observations in
380 mammalian cells, where mitochondrial network fragmentation has been seen to occur in
381 response to mtDNA damage (Ghosh et al., 2019). This suggests that mitochondrial
382 reorganization may be a universal response to mtDNA perturbation, as a fundamental quality
383 control mechanism to deal with mitochondrial dysfunction and regulate mtDNA/
384 mitochondrial segregation as well as clearance. Indeed in metazoans, mitochondrial fission
385 has been proposed to facilitate selective removal and degradation of mitochondria via
386 processes such as PINK-Parkin mediated mitophagy (Ni et al., 2015; Scheibye-Knudsen et al.,
387 2015). Our results instead suggest that mitophagy does not play a significant role in the
388 mtDNA damage response in yeast (in the timescales of our present study), and that quality
389 control mechanisms likely act at the level of mtDNA and its segregation (Fig. S5D). For
390 example, previous reports have shown that budding yeast cells segregate mitochondria

391 asymmetrically based on the activity of the organelle (McFaline-Figueroa et al., 2011; Vevea
392 et al., 2014). Such asymmetry could also passively ensure selective segregation of intact
393 mtDNA copies to daughter cells. Indeed, recent studies demonstrate selective removal or
394 clearance of mutated mtDNA via sensing of local mitochondrial activity as well as
395 downregulation of mitochondrial fusion (Hill et al., 2014; Jakubke et al., 2021; Lieber et al.,
396 2019). It is tempting to speculate that in organisms like budding yeast, that divide
397 asymmetrically, the inability of dysfunctional mitochondria to fuse with the rest of the
398 mitochondrial network, along with selective segregation during division, is the predominant
399 mitochondrial quality control mechanism even in response to mtDNA damage.
400
401 In sum, our study underscores: a. the impact of perturbations to mtDNA integrity on
402 mitochondrial dynamics and function; b. the importance of Mip1 exonuclease activity in
403 mtDNA maintenance under damage and c. the ability of cells to decouple mitochondrial and
404 mtDNA partitioning under mtDNA damage, with an emphasis on mitochondrial maintenance
405 even in the absence of mtDNA, in glycolysis replete conditions. Indeed, the mtDarT system
406 developed here can provide a unique approach to enable future investigations on the
407 mechanisms that govern mtDNA-specific damage repair and recovery across diverse growth
408 conditions.

409 **Materials and methods**:

410 **Yeast strains and growth conditions**

411 A prototrophic strain CEN.PK of *Saccharomyces cerevisiae* was used as the background strain
412 in all the experiments (van Dijken et al., 2000). Plasmids, strains used in the study are listed
413 in Supplementary Table 1-3. Yeast cultures were grown in rich YP media (containing 2%
414 Peptone, 1% Yeast extract, and 2% Dextrose or 3% Glycerol as the carbon source) at 30°C with
415 200 rpm shaking with appropriate concentrations of antibiotics, as required. For all time-
416 course and time-lapse experiments, cells were transformed with the plasmids, and
417 transformants were inoculated in YPDextrose containing NAT and allowed to grow overnight.
418 These cultures were induced with β-estradiol at an O.D.~ 0.2. For induction, β-estradiol
419 (working stock- 50µM, prepared from a stock of 1mM in 100% molecular biology grade
420 ethanol) was added to a final concentration of 100nM, unless mentioned otherwise. We
421 performed our experiments in haploid budding yeast cells, and β-estradiol was maintained in
422 the growth medium throughout.

423 Yeast transformations were done using the LiAc method. For plasmid transformations, cells
424 were plated on YPDextrose plates containing appropriate concentrations of NAT and were
425 allowed to grow for 48 hr at 30°C. *mip1*$^{exo-}$ cells transformed with plasmids, were plated on
426 YPGlycerol plates containing appropriate concentrations of NAT and were allowed to grow
427 for 3 days at 30°C.

428 *mip1*$^{exo-}$ mutant was generated as described earlier (Medeiros et al., 2018). Briefly, we first
429 generated a *mip1Δ* strain which resulted in formation of $\boldsymbol{\rho}^0$ cells. We then introduced a copy
430 of the *mip1* gene containing the mutations D171A and E173A along with a hygromycin
431 selection cassette, at the same locus. Successful transformants containing the mutated copy
432 of the gene were then crossed with the wild type strain of the opposite mating type to
433 reintroduce mtDNA. The diploids were sporulated and tetrads were dissected to obtain $\boldsymbol{\rho}^+$
434 *mip1*$^{exo-}$ cells which were selected using hygromycin and the mating type was confirmed using
435 PCR primers specific for mating type locus. *mip1* gene was sequenced to confirm the presence
436 of the mutations. The strain was maintained on YPGlycerol post dissection to ensure selection
437 of only $\boldsymbol{\rho}^+$ cells; experiments were carried out in YPDextrose.

438

439 **Dot blot assay for ADP ribosylation**

440 For separation of mitochondrial and nuclear DNA, differential centrifugation followed by
441 sucrose gradient based separation was employed to fractionate both the organelles.
442 Mitochondrial fractionation was done as described earlier in (Gregg et al., 2009; Meisinger et
443 al., 2006). DNA was isolated from the nuclear and mitochondrial fractions using a Qiagen
444 DNeasy Blood and Tissue kit.

445 Isolated DNA was then used to perform a dot-blot assay as described in (Jia et al., 2017;
446 Luviano et al., 2018). Briefly, 180ng of each DNA sample was denatured in 0.3M NaOH for 10
447 min at 95˚C. Immediately post denaturation, 5µl (~90ng) of DNA was spotted on nitro cellulose
448 membrane. DNA was then crosslinked to the membrane using a UV-crosslinker at 1200J. The
449 membrane was blocked using 5% blocking solution prepared in TBST for 1 hr at RT, followed
450 by incubation with 1:500 dilution of anti-pan-ADPr-binding reagent (Merck #MABE1016) in
451 TBST for 1 hr at RT. The membrane was then washed thrice with TBST for 10 min each and
452 then probed with 1:5000 dilution of HRP conjugated secondary antibody for 1 hr at RT. After
453 the incubation, the membrane was again washed thrice, 10 min each in TBST and then
454 developed using SuperSignal West PICO PLUS or FEMTO PLUS chemiluminescent substrate.
455 As a loading control, same volumes of samples were also spotted on another membrane,
456 which after crosslinking, was stained with 0.04% of methylene blue prepared in 0.5M Sodium
457 Acetate.

458 **mtDNA and mitochondrial staining**

459 For visualizing mtDNA, a previously described protocol was used (Jajoo et al., 2016). Briefly,
460 1ml of culture was pelleted and washed with 1X PBS. The supernatant was discarded and cells
461 were re- suspended in the residual buffer to give 50µl cell suspension. 0.5µl of undiluted SYBR
462 Green I (Invitrogen) was added to the cell suspension and mixed with gentle tapping. Cells
463 were immediately pelleted and supernatant was discarded. The pellets were washed with
464 1ml of 1X PBS. Cells were subsequently diluted to appropriate densities in 1X PBS before
465 imaging.

466 For visualizing the mitochondrial membrane potential, cells were pelleted and re-suspended
467 in 10ml of YPDextrose media (pre-warmed to 30˚C) containing 1.5µM of TMRE. The cells were

468 incubated in the dark for 20 min in a shaker incubator (30° C, 200 rpm). Subsequently, cells
469 were pelleted down and washed with YPDextrose media in 2X the original volume of culture
470 used for staining. The cell pellets were resuspended to appropriate density in YPDextrose
471 prior to imaging. For time lapses, cells were stained with TMRE post 3.5 hr of induction, in
472 presence of 100nM β- estradiol. Following this, cells were washed and spotted on YPDextrose
473 pads for imaging.

474 **Fluorescence Microscopy**

475 Overnight cultures were allowed to grow till O.D.~0.2. At this O.D, mtDarT expression was
476 induced with 100nM β-estradiol. For time course experiments, samples were spotted on 1%
477 ultra-pure agarose water pads, and for time lapse experiments, samples were spotted on
478 YPDextrose pads with 100nM β-estradiol.

479 Microscopy was performed on a wide-field epifluorescence microscope (Eclipse Ti-2E, Nikon)
480 with a 60X oil immersion objective (plan apochromat objective with NA 1.41) and illumination
481 from pE4000 light source (CoolLED). The microscope was equipped with a motorized XYZ
482 stage and focus was maintained using an infrared-based Perfect Focusing System (Nikon).
483 Image acquisitions were done with Hamamatsu Orca Flash 4.0 camera using NIS-elements
484 software (version 5.1). For time-lapse imaging, samples were placed inside an OkoLab
485 incubation chamber maintained at 30°C and imaged at specific intervals for the indicated
486 period of time.

487 For SIM imaging, coverslips were sequentially washed in methanol and 100% ethanol and
488 flame dried prior to sample preparation. Cells were fixed in 3.7% para-formaldehyde (900µl
489 of cell suspension was added to 100µl of 37% para-formaldehyde) and then washed with 1X
490 PBS. Cells were then spotted on 1% ultra-pure agarose water pads and imaged. Samples were
491 imaged with Nikon 3D-SIM microscope equipped with an ANDOR iXon DU-897 EMCCD camera
492 (512X512), 100X ApoTIRF 1.49 NA oil objective with Coherent Sapphire 561nm solid state
493 laser as the light source. Image reconstruction was done using NIS elements software
494 (Illumination modulation contrast – Auto, High resolution noise suppression – 1X, Out of focus
495 blur suppression – 0.25). During acquisition, 800ms exposure for Cox4-mCherry with 20%
496 laser power, 150 EM gain and 0.3 µm step size was used.

497 **Seahorse assay**

498 Basal respiration rate was estimated by performing seahorse flux assays using Agilent
499 Seahorse XFe24 analyzer. 1 ml of the XF Calibrant solution was aliquoted into each well of the
500 plate and the sensor cartridge plate was hydrated overnight as per the manufacturer's
501 instructions. To adhere the cells to the bottom of the wells, the plate was first coated with
502 poly-L-Lysine for 1 hour at RT. Excess poly-L-lysine was removed and the plate was dried at
503 30°C. Cells grown in YPDextrose media containing appropriate concentration of NAT were
504 induced with 100nM β-estradiol at O.D.~0.2. Cells were serially diluted 4 hr post induction
505 and then aliquoted into the wells such that the final number of cells in each well ~$3X10^5$. The
506 plate was centrifuged at 100g for 2 min and incubated at 30°C for 30 min to allow the cells to
507 adhere to the bottom of the wells. Simultaneously, the sensor cartridge was loaded with 1mM
508 of complex IV inhibitor sodium azide and equilibrated in the Seahorse XFe24 analyzer one
509 hour prior to the start of the assay. The plate was then loaded to the Seahorse XFe24 analyzer
510 and the basal OCR was measured over time. A minimum of two measurements were taken
511 with intermittent 2 min mixing and waiting steps. This was followed by sodium azide injection
512 to the sample wells, and three measurements were taken with intermittent 2 min mixing and
513 waiting steps.

514 **Arrest experiment**

515 Cells transformed with empty vector or mtDarT plasmid were grown overnight in YPG media
516 containing appropriate concentration of NAT. Overnight cultures were allowed to reach early
517 log phase (O.D.~0.2-0.6), after which they were pelleted and resuspended in pre-warmed YPD
518 media (30^0C) containing 20ng/ml of alpha factor with NAT. The cultures were allowed to grow
519 at 30^0C for 2 hr at 200rpm. Simultaneously, separate cultures without alpha factor were also
520 maintained. Following 2 hr, samples were collected for microscopy (SYBR staining) and flow
521 cytometry. Samples were subsequently induced with 100nM β-estradiol. Similarly, samples
522 were collected after 4 hr of induction for microscopy and flow cytometry. (Note: Cells were
523 pelleted and resuspended in fresh media containing alpha factor, 100nM β-estradiol and NAT
524 3 hr post induction to ensure continuous arrest).

525

526 **Image analysis**

527 All image analysis was performed using MATLAB and Fiji (ImageJ) (Schindelin et al., 2012).
528 Mitochondrial analysis was done on 2D maximum projections of z-stacks and images were
529 deconvolved using NIS-elements AR software (Richardson-Lucy algorithm with 60-iterations).
530 Cell segmentation was performed using a MATLAB algorithm (Doncic et al., 2013). Cell
531 outlines were extracted from .mat output files from the algorithm and then ROIs were
532 obtained using Fiji. For segmentation of mitochondria, a custom pipeline was set up in Fiji
533 (briefly involving a. Background subtraction (Rolling ball radius: 50 pixels). b. Sigma Filter Plus
534 (radius =1 pixel, use pixels within = 2 sigmas, Minimum pixel fraction = 0.2). c. Enhanced Local
535 Contrast (CLAHE) (Blocksize = 64, histogram = 256, maximum = 2). d. Tubeness filter (sigma
536 =1.000). e. Images converted to 8-bit. f. Thresholding (10,255) (Minimum threshold was
537 adjusted between 8-15 depending on the quality of segmentation). g. Images converted to
538 mask, Despeckled and Remove outliers (Radius =2, threshold =50)) and the mitochondrial
539 descriptors (Mean form factor, mtArea, Number of mitochondria on per cell basis) were
540 obtained using Mitochondrial analyzer (Chaudhry et al., 2020). Whole cell TMRE intensity was
541 analyzed from maximum projections using 'Measure' in Fiji. For Fig. 2A, cells were manually
542 binned into three morphological categories and buds were excluded from the analysis. For
543 detection of mtDNA foci post SYBR Green I staining, 3D maxima finder plugin (part of the 3D
544 ImageJSuite) in ImageJ was utilized. Since cells with less/without any mtDNA also show
545 nuclear DNA staining, we manually scored these cells post segmentation to account for
546 detection of foci due to nuclear staining. For mtDNA analysis in mother vs bud, pairs without
547 any mtDNA foci (in both cell types) were removed. Mitochondrial volume was analyzed using
548 Mitograph and volume was calculated from the number of voxels detected (Rafelski et al.,
549 2012; Viana et al., 2015). Colocalization of GFP-Atg8 with Cox4-mCherry was scored manually
550 as described in (Böckler & Westermann, 2014). Association of Atg8 foci with mitochondria
551 was checked in the plane of z-stack where GFP-Atg8 intensity was maximum.

552 **Western blotting**

553 Transformants were inoculated in 100-120 ml of YPDextrose with appropriate concentrations
554 of NAT. Cultures were induced with 100nM β-estradiol at an O.D ~ 0.2. Cells were harvested
555 and protein isolation was performed using the Trichloroacetic acid (TCA) extraction method.

556 Pellets were resuspended in 300µl of 10% TCA and lysed by bead beating thrice. The
557 precipitates were resuspended in 200µl of SDS-Glycerol buffer (7.3% SDS, 29.1% glycerol and
558 83.3 mM Tris base) and boiled at 95°C for 10 min with frequent vortexing. The lysate was
559 precipitated and the supernatant was obtained containing protein. Estimation of protein
560 concentration was done using the BCA estimation method using GBioSciences assay kit. The
561 assay was performed in disposable cuvettes, where 5µl was mixed with 1ml Solution A and
562 20µl of Solution B and incubated at 30°C for 30 min. The absorbance was recorded at 565nm.
563 Equal amounts of protein were then loaded on a polyacrylamide gel. For Cox4-mCherry,
564 Dnm1-HA blots 8-10% gels were used. PVDF membranes were used for blotting, which were
565 probed with anti-mCherry (1:5000), anti-HA (1:5000) antibodies, anti-Cox2 (1:1000). HRP
566 conjugated secondary antibodies were used (1:5000) for western blotting and blots were
567 developed using SuperSignal West PICO PLUS or FEMTO PLUS chemiluminescent substrate.
568 Equal amount of proteins was loaded on a separate gel and stained with Coomassie Brillian
569 Blue as a loading control.

570 **Immunocytochemistry**

571 Mid-log phase cells were harvested and fixed in 1ml of 4% paraformaldehyde for 30 min at
572 room temperature. After washing the cells twice with a phosphate-sorbitol buffer (0.1 M
573 KPO4 and 1x in 0.1 M KPO4/1.2 M sorbitol), the pellet was resuspended in 1 ml of 0.1M
574 KPO4/1.2M sorbitol. Cells were then spheroplasted with 10mg/ml Zymolyase for 10-30 min
575 in presence of β-mercaptoethanol. Spheroplasting was checked by imaging cells on the
576 microscope. For imaging, slides/dishes were prepared by washing in chilled methanol and
577 95% ethanol. Slides were then coated with 0.1% Poly-L lysine for 5-10 min and then washed
578 thrice with dH2O. 15µl of spheroplast suspension was placed in each well for 5-10 min at
579 room temperature and then aspirated, and immediately plunged into ice cold methanol for
580 5-6 min and then in cold acetone for 30 sec. Post air drying, 25µl of PBS-BSA was used for
581 blocking. Primary antibody probing was done following 30 min of blocking, for 1 hr. After 5
582 washes with PBS-BSA, secondary antibody was added and incubated for 1-2 hr in a humid
583 chamber in the dark. The wells were again washed with PBS-BSA five times (each wash for 10
584 min) and then twice with only PBS. Slides were mounted with mounted media (Slowfade DAPI
585 reagent) and imaged.

586 **Acknowledgements**

587 The authors are grateful to Dr. Ivan Ahel for sharing bacterial DarT and DarG constructs and
588 Afroze Chimthanawala for assistance with SIM imaging. The authors thank Dr. Sunil Laxman
589 and members of the AB and SL labs for helpful discussions and feedback on the manuscript.
590 This work was supported by fellowships from TIFR (ND), CSIR (AS) as well as grants from HFSP
591 CDA (00051/ 2017-C) (AB) and intramural funding from NCBS-TIFR (AB).
592

593 **Author contributions**

594 ND: conception of project, experimental design, generation of tools and reagents, execution
595 of experiments, data analysis, writing of manuscript. AS: experimental design, generation of
596 tools and reagents, execution of experiments, data analysis, editing of manuscript. AB:
597 conception of project, project supervision, experimental design and writing of manuscript.
598

599 **Declaration of interests**

600 The authors declare no competing interests.
601
602

603 **References**

604 Alexeyev, M., Shokolenko, I., Wilson, G., & LeDoux, S. (2013). The Maintenance of
605 Mitochondrial DNA Integrity—Critical Analysis and Update. *Cold Spring Harbor*
606 *Perspectives in Biology*, *5*(5). https://doi.org/10.1101/cshperspect.a012641
607
608 Bagamery, L. E., Justman, Q. A., Garner, E. C., & Murray, A. W. (2020). A Putative Bet-
609 Hedging Strategy Buffers Budding Yeast against Environmental Instability. *Current Biology*,
610 *30*(23), 4563-4578.e4. https://doi.org/10.1016/j.cub.2020.08.092
611
612 Bleazard, W., McCaffery, J. M., King, E. J., Bale, S., Mozdy, A., Tieu, Q., Nunnari, J., &
613 Shaw, J. M. (1999). The dynamin-related GTPase Dnm1 regulates mitochondrial fission in
614 yeast. *Nature Cell Biology*, *1*(5), 298–304. https://doi.org/10.1038/13014
615
616 Böckler, S., & Westermann, B. (2014). Mitochondrial ER Contacts Are Crucial for Mitophagy
617 in Yeast. *Developmental Cell*, *28*(4), 450–458. https://doi.org/10.1016/j.devcel.2014.01.012
618
619 Boesch, P., Weber-Lotfi, F., Ibrahim, N., Tarasenko, V., Cosset, A., Paulus, F., Lightowlers,
620 R. N., & Dietrich, A. (2011). DNA repair in organelles: Pathways, organization, regulation,
621 relevance in disease and aging. *Biochimica et Biophysica Acta (BBA) - Molecular Cell*
622 *Research*, *1813*(1), 186–200. https://doi.org/10.1016/j.bbamcr.2010.10.002
623
624 Breeden, L. L. (1997). α-Factor synchronization of budding yeast. In *Methods in Enzymology*
625 (Vol. 283, pp. 332–342). Academic Press. https://doi.org/10.1016/S0076-6879(97)83027-3
626
627 Brown, T. A., Tkachuk, A. N., Shtengel, G., Kopek, B. G., Bogenhagen, D. F., Hess, H. F., &
628 Clayton, D. A. (2011). Superresolution Fluorescence Imaging of Mitochondrial Nucleoids
629 Reveals Their Spatial Range, Limits, and Membrane Interaction. *Molecular and Cellular*
630 *Biology*. https://doi.org/10.1128/MCB.05694-11
631
632 Burman, J. L., Pickles, S., Wang, C., Sekine, S., Vargas, J. N. S., Zhang, Z., Youle, A. M.,
633 Nezich, C. L., Wu, X., Hammer, J. A., & Youle, R. J. (2017). Mitochondrial fission facilitates
634 the selective mitophagy of protein aggregates. *Journal of Cell Biology*, *216*(10), 3231–3247.
635 https://doi.org/10.1083/jcb.201612106
636
637 Busch, K. B., Kowald, A., & Spelbrink, J. N. (2014). Quality matters: How does mitochondrial
638 network dynamics and quality control impact on mtDNA integrity? *Philosophical*
639 *Transactions of the Royal Society B: Biological Sciences*, *369*(1646), 20130442.
640 https://doi.org/10.1098/rstb.2013.0442
641
642 Chaudhry, A., Shi, R., & Luciani, D. S. (2020). A pipeline for multidimensional confocal
643 analysis of mitochondrial morphology, function, and dynamics in pancreatic β-cells. *American*
644 *Journal of Physiology-Endocrinology and Metabolism*, *318*(2), E87–E101.
645 https://doi.org/10.1152/ajpendo.00457.2019
646
647 Chen, X. J., & Butow, R. A. (2005). The organization and inheritance of the mitochondrial
648 genome. *Nature Reviews Genetics*, *6*(11), 815–825. https://doi.org/10.1038/nrg1708
649

650 Clayton, D. A., Doda, J. N., & Friedberg, E. C. (1974). The Absence of a Pyrimidine Dimer
651 Repair Mechanism in Mammalian Mitochondria. *Proceedings of the National Academy of*
652 *Sciences of the United States of America*, *71*(7), 2777–2781.
653
654 Detmer, S. A., & Chan, D. C. (2007). Functions and dysfunctions of mitochondrial dynamics.
655 *Nature Reviews Molecular Cell Biology*, *8*(11), 870–879. https://doi.org/10.1038/nrm2275
656
657 Doncic, A., Eser, U., Atay, O., & Skotheim, J. M. (2013). An Algorithm to Automate Yeast
658 Segmentation and Tracking. *PLOS ONE*, *8*(3), e57970.
659 https://doi.org/10.1371/journal.pone.0057970
660
661 Duvezin-Caubet, S., Jagasia, R., Wagener, J., Hofmann, S., Trifunovic, A., Hansson, A.,
662 Chomyn, A., Bauer, M. F., Attardi, G., Larsson, N.-G., Neupert, W., & Reichert, A. S. (2006).
663 Proteolytic Processing of OPA1 Links Mitochondrial Dysfunction to Alterations in
664 Mitochondrial Morphology *. *Journal of Biological Chemistry*, *281*(49), 37972–37979.
665 https://doi.org/10.1074/jbc.M606059200
666
667 Ephrussi, B., de Margerie-Hottinguer, H., & Roman, H. (1955). SUPPRESSIVENESS: A
668 NEW FACTOR IN THE GENETIC DETERMINISM OF THE SYNTHESIS OF
669 RESPIRATORY ENZYMES IN YEAST. *Proceedings of the National Academy of Sciences*
670 *of the United States of America*, *41*(12), 1065–1071.
671
672 Farge, G., Laurens, N., Broekmans, O. D., van den Wildenberg, S. M. J. L., Dekker, L. C. M.,
673 Gaspari, M., Gustafsson, C. M., Peterman, E. J. G., Falkenberg, M., & Wuite, G. J. L. (2012).
674 Protein sliding and DNA denaturation are essential for DNA organization by human
675 mitochondrial transcription factor A. *Nature Communications*, *3*(1), 1013.
676 https://doi.org/10.1038/ncomms2001
677
678 Fontanesi, F., Soto, I. C., Horn, D., & Barrientos, A. (2006). Assembly of mitochondrial
679 cytochrome c-oxidase, a complicated and highly regulated cellular process. *American Journal*
680 *of Physiology-Cell Physiology*, *291*(6), C1129–C1147.
681 https://doi.org/10.1152/ajpcell.00233.2006
682
683 Foury, F., & Vanderstraeten, S. (1992). Yeast mitochondrial DNA mutators with deficient
684 proofreading exonucleolytic activity. *The EMBO Journal*, *11*(7), 2717–2726.
685
686 Ghosh, A., Bhattacharjee, S., Chowdhuri, S. P., Mallick, A., Rehman, I., Basu, S., & Das, B.
687 B. (2019). SCAN1-TDP1 trapping on mitochondrial DNA promotes mitochondrial dysfunction
688 and mitophagy. *Science Advances*, *5*(11), eaax9778. https://doi.org/10.1126/sciadv.aax9778
689
690 Gregg, C., Kyryakov, P., & Titorenko, V. I. (2009). Purification of Mitochondria from Yeast
691 Cells. *Journal of Visualized Experiments : JoVE*, *30*, 1417. https://doi.org/10.3791/1417
692
693 Hahn, A., & Zuryn, S. (2019). The Cellular Mitochondrial Genome Landscape in Disease.
694 *Trends in Cell Biology*, *29*(3), 227–240. https://doi.org/10.1016/j.tcb.2018.11.004
695
696 Harwig, M. C., Viana, M. P., Egner, J. M., Harwig, J. J., Widlansky, M. E., Rafelski, S. M., &
697 Hill, R. B. (2018). Methods for imaging mammalian mitochondrial morphology: A prospective
698 on MitoGraph. *Analytical Biochemistry*. https://doi.org/10.1016/j.ab.2018.02.022
699

Herrmann, J. M., & Funes, S. (2005). Biogenesis of cytochrome oxidase-sophisticated assembly lines in the mitochondrial inner membrane. *Gene*, *354*, 43–52. https://doi.org/10.1016/j.gene.2005.03.017

Hill, J. H., Chen, Z., & Xu, H. (2014). Selective propagation of functional mitochondrial DNA during oogenesis restricts the transmission of a deleterious mitochondrial variant. *Nature Genetics*, *46*(4), 389–392. https://doi.org/10.1038/ng.2920

Horie, C., Suzuki, H., Sakaguchi, M., & Mihara, K. (2003). Targeting and Assembly of Mitochondrial Tail-anchored Protein Tom5 to the TOM Complex Depend on a Signal Distinct from That of Tail-anchored Proteins Dispersed in the Membrane *. *Journal of Biological Chemistry*, *278*(42), 41462–41471. https://doi.org/10.1074/jbc.M307047200

Jajoo, R., Jung, Y., Huh, D., Viana, M. P., Rafelski, S. M., Springer, M., & Paulsson, J. (2016). Accurate concentration control of mitochondria and nucleoids. *Science (New York, N.Y.)*, *351*(6269), 169–172. https://doi.org/10.1126/science.aaa8714

Jakubke, C., Roussou, R., Maiser, A., Schug, C., Thoma, F., Bunk, D., Hörl, D., Leonhardt, H., Walter, P., Klecker, T., & Osman, C. (n.d.). Cristae-dependent quality control of the mitochondrial genome. *Science Advances*, *7*(36), eabi8886. https://doi.org/10.1126/sciadv.abi8886

Jankevicius, G., Ariza, A., Ahel, M., & Ahel, I. (2016). The Toxin-Antitoxin System DarTG Catalyzes Reversible ADP-Ribosylation of DNA. *Molecular Cell*, *64*(6), 1109–1116. https://doi.org/10.1016/j.molcel.2016.11.014

Jia, Z., Liang, Y., Ma, B., Xu, X., Xiong, J., Duan, L., & Wang, D. (2017). A 5-mC Dot Blot Assay Quantifying the DNA Methylation Level of Chondrocyte Dedifferentiation In Vitro. *JoVE (Journal of Visualized Experiments)*, *123*, e55565. https://doi.org/10.3791/55565

Jiao, H., Jiang, D., Hu, X., Du, W., Ji, L., Yang, Y., Li, X., Sho, T., Wang, X., Li, Y., Wu, Y.-T., Wei, Y.-H., Hu, X., & Yu, L. (2021). Mitocytosis, a migrasome-mediated mitochondrial quality-control process. *Cell*, *184*(11), 2896-2910.e13. https://doi.org/10.1016/j.cell.2021.04.027

Jin, S. M., & Youle, R. J. (2012). PINK1- and Parkin-mediated mitophagy at a glance. *Journal of Cell Science*, *125*(4), 795–799. https://doi.org/10.1242/jcs.093849

Kanki, T., & Klionsky, D. J. (2008). Mitophagy in Yeast Occurs through a Selective Mechanism. *The Journal of Biological Chemistry*, *283*(47), 32386–32393. https://doi.org/10.1074/jbc.M802403200

Karbowski, M., Arnoult, D., Chen, H., Chan, D. C., Smith, C. L., & Youle, R. J. (2004). Quantitation of mitochondrial dynamics by photolabeling of individual organelles shows that mitochondrial fusion is blocked during the Bax activation phase of apoptosis. *Journal of Cell Biology*, *164*(4), 493–499. https://doi.org/10.1083/jcb.200309082

Kleele, T., Rey, T., Winter, J., Zaganelli, S., Mahecic, D., Perreten Lambert, H., Ruberto, F. P., Nemir, M., Wai, T., Pedrazzini, T., & Manley, S. (2021). Distinct fission signatures predict

749 mitochondrial degradation or biogenesis. *Nature*, *593*(7859), 435–439.
750 https://doi.org/10.1038/s41586-021-03510-6
751
752 Laporte, D., Gouleme, L., Jimenez, L., Khemiri, I., & Sagot, I. (2018). Mitochondria
753 reorganization upon proliferation arrest predicts individual yeast cell fate. *ELife*, *7*, e35685.
754 https://doi.org/10.7554/eLife.35685
755
756 Lawarée, E., Jankevicius, G., Cooper, C., Ahel, I., Uphoff, S., & Tang, C. M. (2020). DNA
757 ADP-Ribosylation Stalls Replication and Is Reversed by RecF-Mediated Homologous
758 Recombination and Nucleotide Excision Repair. *Cell Reports*, *30*(5), 1373-1384.e4.
759 https://doi.org/10.1016/j.celrep.2020.01.014
760
761 Legros, F., Malka, F., Frachon, P., Lombès, A., & Rojo, M. (2004). Organization and dynamics
762 of human mitochondrial DNA. *Journal of Cell Science*, *117*(13), 2653–2662.
763 https://doi.org/10.1242/jcs.01134
764
765 Lewis, S. C., Uchiyama, L. F., & Nunnari, J. (2016). ER-mitochondria contacts couple mtDNA
766 synthesis with mitochondrial division in human cells. *Science*, *353*(6296).
767 https://doi.org/10.1126/science.aaf5549
768
769 Lieber, T., Jeedigunta, S. P., Palozzi, J. M., Lehmann, R., & Hurd, T. R. (2019). Mitochondrial
770 fragmentation drives selective removal of deleterious mtDNA in the germline. *Nature*,
771 *570*(7761), 380–384. https://doi.org/10.1038/s41586-019-1213-4
772
773 Ling, F., Bradshaw, E., & Yoshida, M. (2019). Prevention of mitochondrial genomic instability
774 in yeast by the mitochondrial recombinase Mhr1. *Scientific Reports*, *9*(1), 5433.
775 https://doi.org/10.1038/s41598-019-41699-9
776
777 Lisby, M., Barlow, J. H., Burgess, R. C., & Rothstein, R. (2004). Choreography of the DNA
778 Damage Response: Spatiotemporal Relationships among Checkpoint and Repair Proteins. *Cell*,
779 *118*(6), 699–713. https://doi.org/10.1016/j.cell.2004.08.015
780
781 Louvion, J. F., Havaux-Copf, B., & Picard, D. (1993). Fusion of GAL4-VP16 to a steroid-
782 binding domain provides a tool for gratuitous induction of galactose-responsive genes in yeast.
783 *Gene*, *131*(1), 129–134. https://doi.org/10.1016/0378-1119(93)90681-r
784
785 Ludovico, P., Sansonetty, F., & Côrte-Real, M. (2001). Assessment of mitochondrial
786 membrane potential in yeast cell populations by flow cytometry. *Microbiology (Reading,*
787 *England)*, *147*(Pt 12), 3335–3343. https://doi.org/10.1099/00221287-147-12-3335
788
789 Luviano, N., Diaz-Palma, S., Cosseau, C., & Grunau, C. (2018). *A simple Dot Blot Assay for*
790 *population scale screening of DNA methylation* [Preprint]. Ecology.
791 https://doi.org/10.1101/454439
792
793 McFaline-Figueroa, J. R., Vevea, J., Swayne, T. C., Zhou, C., Liu, C., Leung, G., Boldogh, I.
794 R., & Pon, L. A. (2011). Mitochondrial quality control during inheritance is associated with
795 lifespan and mother-daughter age asymmetry in budding yeast. *Aging Cell*, *10*(5), 885–895.
796 https://doi.org/10.1111/j.1474-9726.2011.00731.x
797

Medeiros, T. C., Thomas, R. L., Ghillebert, R., & Graef, M. (2018). Autophagy balances mtDNA synthesis and degradation by DNA polymerase POLG during starvation. *Journal of Cell Biology*, *217*(5), 1601–1611. https://doi.org/10.1083/jcb.201801168

Meisinger, C., Pfanner, N., & Truscott, K. N. (2006). Isolation of yeast mitochondria. *Methods in Molecular Biology (Clifton, N.J.)*, *313*, 33–39. https://doi.org/10.1385/1-59259-958-3:033

Melo, J. A., Cohen, J., & Toczyski, D. P. (2001). Two checkpoint complexes are independently recruited to sites of DNA damage in vivo. *Genes & Development*, *15*(21), 2809–2821. https://doi.org/10.1101/gad.903501

Nakada, K., Inoue, K., Ono, T., Isobe, K., Ogura, A., Goto, Y. I., Nonaka, I., & Hayashi, J. I. (2001). Inter-mitochondrial complementation: Mitochondria-specific system preventing mice from expression of disease phenotypes by mutant mtDNA. *Nature Medicine*, *7*(8), 934–940. https://doi.org/10.1038/90976

Ni, H.-M., Williams, J. A., & Ding, W.-X. (2015). Mitochondrial dynamics and mitochondrial quality control. *Redox Biology*, *4*, 6–13. https://doi.org/10.1016/j.redox.2014.11.006

Nissanka, N., Bacman, S. R., Plastini, M. J., & Moraes, C. T. (2018). The mitochondrial DNA polymerase gamma degrades linear DNA fragments precluding the formation of deletions. *Nature Communications*, *9*(1), 2491. https://doi.org/10.1038/s41467-018-04895-1

Osman, C., Noriega, T. R., Okreglak, V., Fung, J. C., & Walter, P. (2015). Integrity of the yeast mitochondrial genome, but not its distribution and inheritance, relies on mitochondrial fission and fusion. *Proceedings of the National Academy of Sciences of the United States of America*, *112*(9), E947–E956. https://doi.org/10.1073/pnas.1501737112

Pascucci, B., Versteegh, A., van Hoffen, A., van Zeeland, A. A., Mullenders, L. H., & Dogliotti, E. (1997). DNA repair of UV photoproducts and mutagenesis in human mitochondrial DNA. *Journal of Molecular Biology*, *273*(2), 417–427. https://doi.org/10.1006/jmbi.1997.1268

Peeva, V., Blei, D., Trombly, G., Corsi, S., Szukszto, M. J., Rebelo-Guiomar, P., Gammage, P. A., Kudin, A. P., Becker, C., Altmüller, J., Minczuk, M., Zsurka, G., & Kunz, W. S. (2018). Linear mitochondrial DNA is rapidly degraded by components of the replication machinery. *Nature Communications*, *9*(1), 1727. https://doi.org/10.1038/s41467-018-04131-w

Perlman, P. S. (1976). Genetic analysis of petite mutants of Saccharomyces cerevisiae: Transmissional types. *Genetics*, *82*(4), 645–663. https://doi.org/10.1093/genetics/82.4.645

Pickles, S., Vigié, P., & Youle, R. J. (2018). Mitophagy and Quality Control Mechanisms in Mitochondrial Maintenance. *Current Biology: CB*, *28*(4), R170–R185. https://doi.org/10.1016/j.cub.2018.01.004

Rafelski, S. M., Viana, M. P., Zhang, Y., Chan, Y.-H. M., Thorn, K. S., Yam, P., Fung, J. C., Li, H., Costa, L. da F., & Marshall, W. F. (2012). Mitochondrial Network Size Scaling in Budding Yeast. *Science (New York, N.Y.)*, *338*(6108), 822–824. https://doi.org/10.1126/science.1225720

Ramos, E. S., Motori, E., Brüser, C., Kühl, I., Yeroslaviz, A., Ruzzenente, B., Kauppila, J. H. K., Busch, J. D., Hultenby, K., Habermann, B. H., Jakobs, S., Larsson, N.-G., & Mourier, A. (2019). Mitochondrial fusion is required for regulation of mitochondrial DNA replication. *PLOS Genetics*, *15*(6), e1008085. https://doi.org/10.1371/journal.pgen.1008085

Richter, C. (1995). Oxidative damage to mitochondrial DNA and its relationship to ageing. *The International Journal of Biochemistry & Cell Biology*, *27*(7), 647–653. https://doi.org/10.1016/1357-2725(95)00025-K

Rosebrock, A. P. (2017). Synchronization and Arrest of the Budding Yeast Cell Cycle Using Chemical and Genetic Methods. *Cold Spring Harbor Protocols*, *2017*(1), pdb.prot088724. https://doi.org/10.1101/pdb.prot088724

Scheibye-Knudsen, M., Fang, E. F., Croteau, D. L., Wilson, D. M., & Bohr, V. A. (2015). Protecting the Mitochondrial Powerhouse. *Trends in Cell Biology*, *25*(3), 158–170. https://doi.org/10.1016/j.tcb.2014.11.002

Schindelin, J., Arganda-Carreras, I., Frise, E., Kaynig, V., Longair, M., Pietzsch, T., Preibisch, S., Rueden, C., Saalfeld, S., Schmid, B., Tinevez, J.-Y., White, D. J., Hartenstein, V., Eliceiri, K., Tomancak, P., & Cardona, A. (2012). Fiji: An open-source platform for biological-image analysis. *Nature Methods*, *9*(7), 676–682. https://doi.org/10.1038/nmeth.2019

Schuller, M., Butler, R. E., Ariza, A., Tromans-Coia, C., Jankevicius, G., Claridge, T. D. W., Kendall, S. L., Goh, S., Stewart, G. R., & Ahel, I. (2021). Molecular basis for DarT ADP-ribosylation of a DNA base. *Nature*, *596*(7873), 597–602. https://doi.org/10.1038/s41586-021-03825-4

Scott, I., & Youle, R. J. (2010). Mitochondrial fission and fusion. *Essays in Biochemistry*, *47*, 85–98. https://doi.org/10.1042/bse0470085

Shaw, J. M., & Nunnari, J. (2002). Mitochondrial dynamics and division in budding yeast. *Trends in Cell Biology*, *12*(4), 178–184.

Shokolenko, I. N., Wilson, G. L., & Alexeyev, M. F. (2013). Persistent damage induces mitochondrial DNA degradation. *DNA Repair*, *12*(7), 488–499. https://doi.org/10.1016/j.dnarep.2013.04.023

Song, Z., Chen, H., Fiket, M., Alexander, C., & Chan, D. C. (2007). OPA1 processing controls mitochondrial fusion and is regulated by mRNA splicing, membrane potential, and Yme1L. *Journal of Cell Biology*, *178*(5), 749–755. https://doi.org/10.1083/jcb.200704110

Stevnsner, T., Thorslund, T., de Souza-Pinto, N. C., & Bohr, V. A. (2002). Mitochondrial repair of 8-oxoguanine and changes with aging. *Experimental Gerontology*, *37*(10–11), 1189–1196. https://doi.org/10.1016/s0531-5565(02)00142-0

Stuart, J. A., Mayard, S., Hashiguchi, K., Souza-Pinto, N. C., & Bohr, V. A. (2005). Localization of mitochondrial DNA base excision repair to an inner membrane-associated particulate fraction. *Nucleic Acids Research*, *33*(12), 3722–3732. https://doi.org/10.1093/nar/gki683

Swartzlander, D. B., Griffiths, L. M., Lee, J., Degtyareva, N. P., Doetsch, P. W., & Corbett, A. H. (2010). Regulation of base excision repair: Ntg1 nuclear and mitochondrial dynamic localization in response to genotoxic stress. *Nucleic Acids Research*, *38*(12), 3963–3974. https://doi.org/10.1093/nar/gkq108

Taylor, R. W., & Turnbull, D. M. (2005). Mitochondrial DNA mutations in human disease. *Nature Reviews Genetics*, *6*(5), 389–402. https://doi.org/10.1038/nrg1606

Thyagarajan, B., Padua, R. A., & Campbell, C. (1996). Mammalian mitochondria possess homologous DNA recombination activity. *The Journal of Biological Chemistry*, *271*(44), 27536–27543. https://doi.org/10.1074/jbc.271.44.27536

Torggler, R., Papinski, D., & Kraft, C. (2017). Assays to Monitor Autophagy in Saccharomyces cerevisiae. *Cells*, *6*(3), E23. https://doi.org/10.3390/cells6030023

Twig, G., Elorza, A., Molina, A. J. A., Mohamed, H., Wikstrom, J. D., Walzer, G., Stiles, L., Haigh, S. E., Katz, S., Las, G., Alroy, J., Wu, M., Py, B. F., Yuan, J., Deeney, J. T., Corkey, B. E., & Shirihai, O. S. (2008). Fission and selective fusion govern mitochondrial segregation and elimination by autophagy. *The EMBO Journal*, *27*(2), 433–446. https://doi.org/10.1038/sj.emboj.7601963

van Dijken, J. P., Bauer, J., Brambilla, L., Duboc, P., Francois, J. M., Gancedo, C., Giuseppin, M. L. F., Heijnen, J. J., Hoare, M., Lange, H. C., Madden, E. A., Niederberger, P., Nielsen, J., Parrou, J. L., Petit, T., Porro, D., Reuss, M., van Riel, N., Rizzi, M., … Pronk, J. T. (2000). An interlaboratory comparison of physiological and genetic properties of four Saccharomyces cerevisiae strains. *Enzyme and Microbial Technology*, *26*(9), 706–714. https://doi.org/10.1016/S0141-0229(00)00162-9

Vevea, J. D., Swayne, T. C., Boldogh, I. R., & Pon, L. A. (2014). Inheritance of the fittest mitochondria in yeast. *Trends in Cell Biology*, *24*(1). https://doi.org/10.1016/j.tcb.2013.07.003

Viana, M. P., Lim, S., & Rafelski, S. M. (2015). Quantifying mitochondrial content in living cells. *Methods in Cell Biology*, *125*, 77–93. https://doi.org/10.1016/bs.mcb.2014.10.003

Wallace, D. C. (2010). Mitochondrial DNA mutations in disease and aging. *Environmental and Molecular Mutagenesis*, *51*(5), 440–450. https://doi.org/10.1002/em.20586

Westermann, B. (2008). Molecular Machinery of Mitochondrial Fusion and Fission. *Journal of Biological Chemistry*, *283*(20), 13501–13505. https://doi.org/10.1074/jbc.R800011200

Westermann, B. (2010). Mitochondrial fusion and fission in cell life and death. *Nature Reviews Molecular Cell Biology*, *11*(12), 872–884. https://doi.org/10.1038/nrm3013

Westermann, B. (2014). Mitochondrial inheritance in yeast. *Biochimica Et Biophysica Acta*, *1837*(7), 1039–1046. https://doi.org/10.1016/j.bbabio.2013.10.005

Yakes, F. M., & Van Houten, B. (1997). Mitochondrial DNA damage is more extensive and persists longer than nuclear DNA damage in human cells following oxidative stress. *Proceedings of the National Academy of Sciences of the United States of America*, *94*(2), 514–519. https://doi.org/10.1073/pnas.94.2.51

Zhang, Y., Wang, Z.-H., Liu, Y., Chen, Y., Sun, N., Gucek, M., Zhang, F., & Xu, H. (2019). PINK1 Inhibits Local Protein Synthesis to Limit Transmission of Deleterious Mitochondrial DNA Mutations. *Molecular Cell*, *73*(6), 1127-1137.e5. https://doi.org/10.1016/j.molcel.2019.01.013

954 **Main Figure legends**

955 **Figure 1: System to induce mitochondria-specific DNA damage.** (A). Schematic representing
956 expression and localization of mtDarT on addition of β-estradiol (Left panel); Diagrammatic
957 representation of ADP-ribosylation of single-stranded DNA in presence of DarT and NAD+
958 (Right panel). (B). Immunostaining for FLAG-tagged mtDarT/TE160A in cells expressing
959 mitochondrially-targeted mNeongreen. Intensity line profiles for mtDarT and mNeonGreen
960 are show at the bottom. (Scale bar-5µm, white dotted lines mark cell outlines, here and in all
961 other images) (C). Cell survival under increasing concentrations of β-estradiol on plates
962 containing either dextrose or glycerol as a carbon source; cells were transformed with
963 plasmids expressing mtDarT/TE160A or empty vector as a control. (D). Dot blot assay to assess
964 ADP ribosylation on DNA, upon mtDarT expression. Both mitochondrial and nuclear DNA is
965 probed. As a loading control, same volumes of samples were spotted on a separate
966 membrane and stained with 0.04% of methylene blue

967 **Figure 2: mtDNA damage impacts mitochondrial organization and dynamics.** (A).
968 Representative cells showing three categories of mitochondrial morphologies observed (left
969 panel); Percentage of cells in each category in control (empty vector) or mtDarT cells after 8
970 hr of induction (Mean ± SD from three biological replicates, n>150 in each replicate) (right
971 panel). (B). Cells expressing Cox4::mCherry imaged in widefield and SIM mode, with
972 representative cells showing tubular and fragmented mitochondrial morphologies after 6 hr
973 of induction with 100nM β-estradiol. (C). Two parameters: - Mean form factor (MFF) and
974 number of mitochondria are used to quantify mitochondrial morphologies in the population.
975 Details on calculation of MFF is provided, along with a diagrammatic representation of
976 possible mitochondrial organizations observed in the 2D density plots (D). Density plots with
977 Mean form factor and number of mitochondria over time; n>680 in each plot, from 3
978 biological replicates. (E). Montage of cells with Cox4::mCherry, imaged every 5 min for 40 min,
979 after 4 hr of induction with β-estradiol; mitochondrial morphology at the start of the
980 experiment is indicated. T0 refers to the frame at the start of the imaging (after the period of
981 pre-induction) here and in Fig. 2F. (F). Density plots with Mean form factor and number of
982 mitochondria over time, plotted for cells starting with MFF<2 at the beginning of time lapse;
983 n=84 for empty vector, n= 151 for mtDarT pooled from 3 biological replicates.

984 **Figure 3: mtDNA damage results in mitochondrial dysfunction.** (A). Representative images
985 of cells expressing Cox4::GFP and stained with TMRE after 8 hr of induction with β-estradiol
986 (left panel). Total TMRE intensity normalized to cell area is plotted (n>1030 from 3 biological
987 replicates) (right panel). (B). Schematic of experimental design for time lapse experiment in
988 Fig. 3C-D. (C) Montage of cells expressing mt-mNeongreen stained with TMRE tracked over
989 time, imaged every 5 min for 40 min. TMRE was imaged only at t=0 of time lapse. T0 refers to
990 the frame at the start of the imaging (after the period of pre-induction). (D) Scatter plot with
991 Mean form factor and number of mitochondria over time, plotted for cells starting with
992 MFF<2 at the beginning of time lapse. Each data point represents one cell with colour
993 corresponding to TMRE intensity normalized to cell area at t=0 min; n=61 for empty vector,
994 n=91 for mtDarT from 3 biological replicates. Statistical significance in A was calculated using
995 Mann-Whitney U test. (*** p<0.0001, ** p<0.005, * p< 0.05, n.s.- not significant, in all cases).

996 **Figure 4: Changes in mitochondrial morphology accompany loss of mtDNA but not**
997 **mitochondria.** (A). Montage of cells expressing Cox4::mCherry stained with SYBR Green I to
998 visualize mtDNA over time. (B). Percentage of cells over time without any mtDNA foci. Mean
999 ± SD from 3 biological replicates; n>100 in each biological replicate. (C). Cox4::mCherry and
1000 Tom20::mCherry western blot with quantification from 3 biological replicates, normalized to
1001 empty vector at t=0; Error bars: SD. Statistical significance in C was calculated using unpaired
1002 Student's t-test.

1003 **Figure 5: Exonuclease activity of the mtDNA polymerase, Mip1, is essential for mtDNA**
1004 **maintenance.** (A) Schematic showing domain organization of Mip1, with amino acid
1005 mutations for *mip1*$^{exo-}$ marked in red (D171A, E173A). (B) Percentage of cells over time
1006 without any mtDNA foci (p^0) are plotted. Mean ± SD from three biological replicates; n>85 in
1007 each biological replicate. (C) Representative images of *mip1*$^{exo-}$ cells expressing
1008 Cox4::mCherry stained with SYBR Green I. Yellow arrows mark mitochondria devoid of
1009 mtDNA. (D-E). Fraction of mtDNA in bud (number of mtDNA foci in bud/total number of
1010 mtDNA foci in the mother-bud pair) is plotted against fraction cell area (area of the bud/total
1011 area of the mother-bud pair) for both wild type and *mip1*$^{exo-}$ cells, after 4 hr (top panel) or 6
1012 hr of induction (bottom panel). Black line represents mean and shaded region represents SD
1013 (calculated after binning x-axis in bins of 0.05). R^2 values were obtained via Pearson's
1014 Correlation; n>145 from 4 biological replicates for *mip1*$^{exo-}$ and 3 biological replicates for wild

1015 type. Statistical significance in E was calculated using Fisher's F-test, applied on distributions
1016 of residual values of all data points (distance from linear fit curve). Comparisons were made
1017 to empty vector control of corresponding time point. (F) Schematic of experimental design to
1018 arrest cells, followed by SYBR staining at 0 and 4 hr of induction. Flow cytometry profiles
1019 corresponding to the time point are shown at the bottom (left); percentage cells without
1020 mtDNA foci in wild type and *mip1*$^{exo-}$ cells expressing mtDarT (right). N>670 cells from 3
1021 biological replicates.

Figure 1

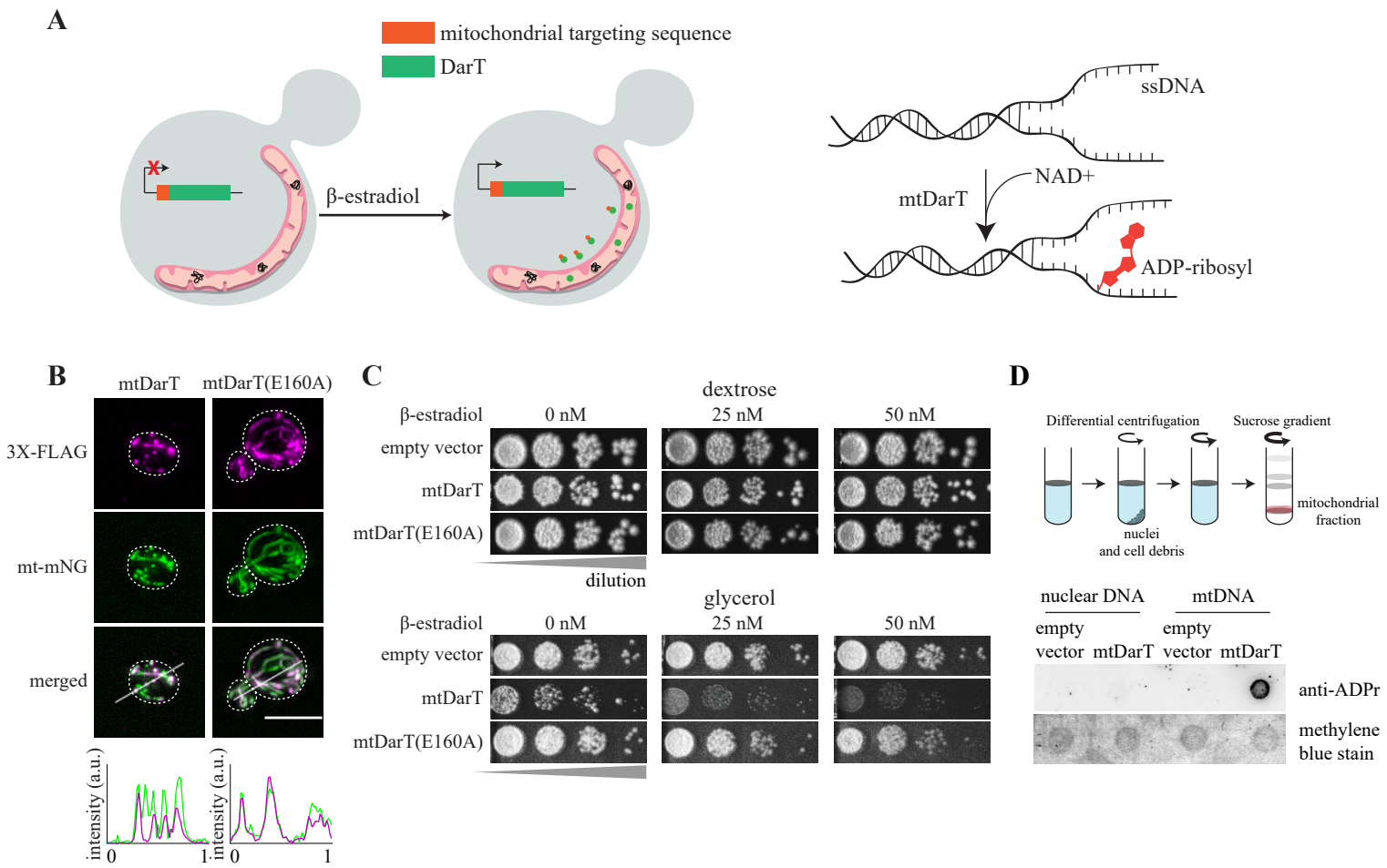
A
mitochondrial targeting sequence
DarT
β-estradiol
ssDNA
NAD+
mtDarT
ADP-ribosyl
B
mtDarT
mtDarT(E160A)
3X-FLAG
mt-mNG
merged
intensity (a.u.)
0
1
C
dextrose
β-estradiol
0 nM
25 nM
50 nM
empty vector
mtDarT
mtDarT(E160A)
dilution
glycerol
D
Differential centrifugation
Sucrose gradient
nuclei
and cell debris
mitochondrial
fraction
nuclear DNA
mtDNA
empty
vector
mtDarT
anti-ADPr
methylene
blue stain

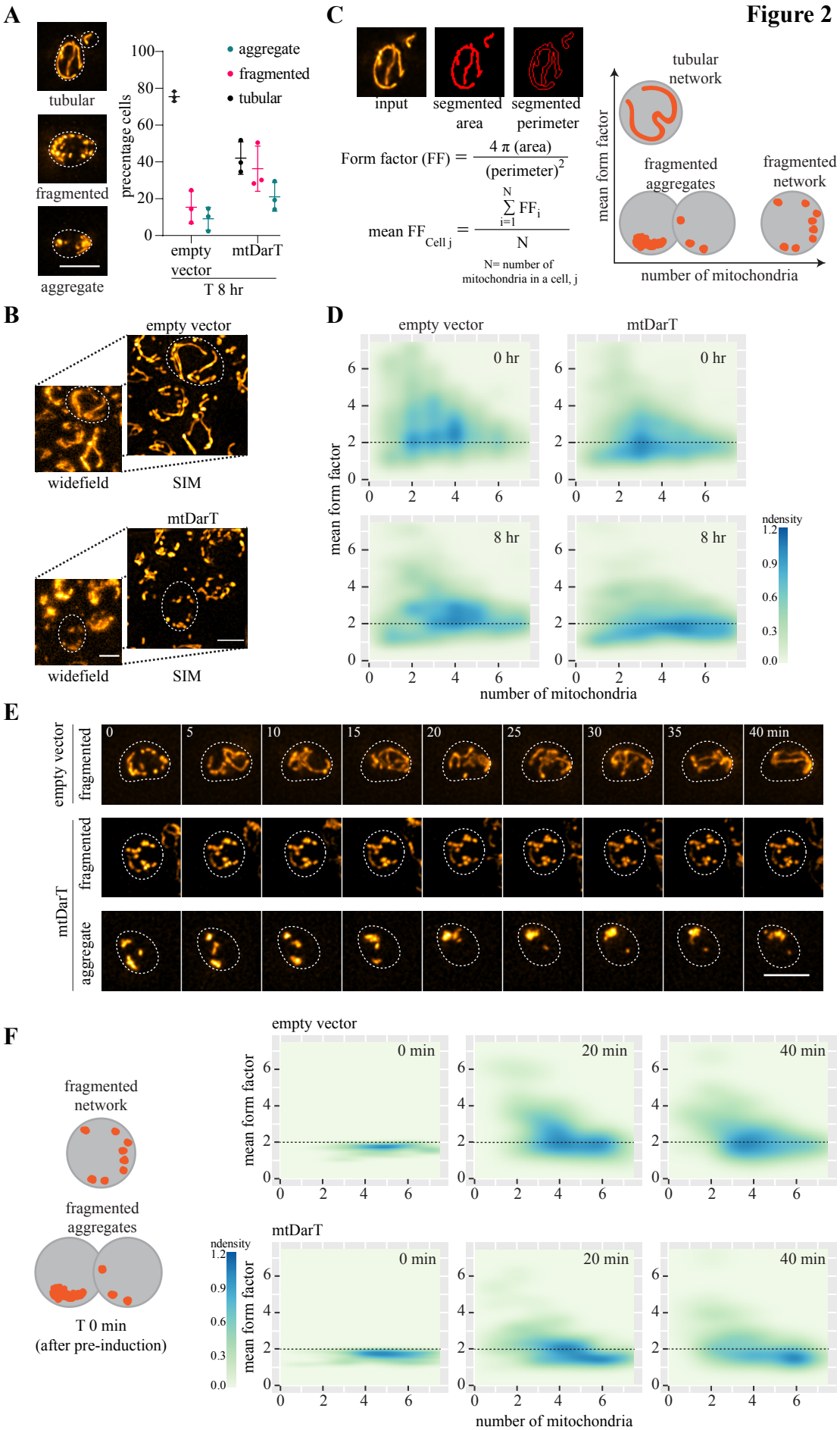

Figure 2
A
tubular
fragmented
aggregate
precentage cells
aggregate
fragmented
tubular
empty vector
mtDarT
T 8 hr
B
empty vector
widefield
SIM
mtDarT
widefield
SIM
C
input
segmented area
segmented perimeter
Form factor (FF) = 4 π (area) / (perimeter)^2
mean FF Cell j = Σ FFi / N
N= number of mitochondria in a cell, j
tubular network
fragmented aggregates
fragmented network
mean form factor
number of mitochondria
D
empty vector
mtDarT
0 hr
8 hr
mean form factor
number of mitochondria
ndensity
E
empty vector
fragmented
mtDarT
fragmented
aggregate
0
5
10
15
20
25
30
35
40 min
F
fragmented network
fragmented aggregates
T 0 min
(after pre-induction)
empty vector
mtDarT
0 min
20 min
40 min
mean form factor
number of mitochondria
ndensity

Figure 3

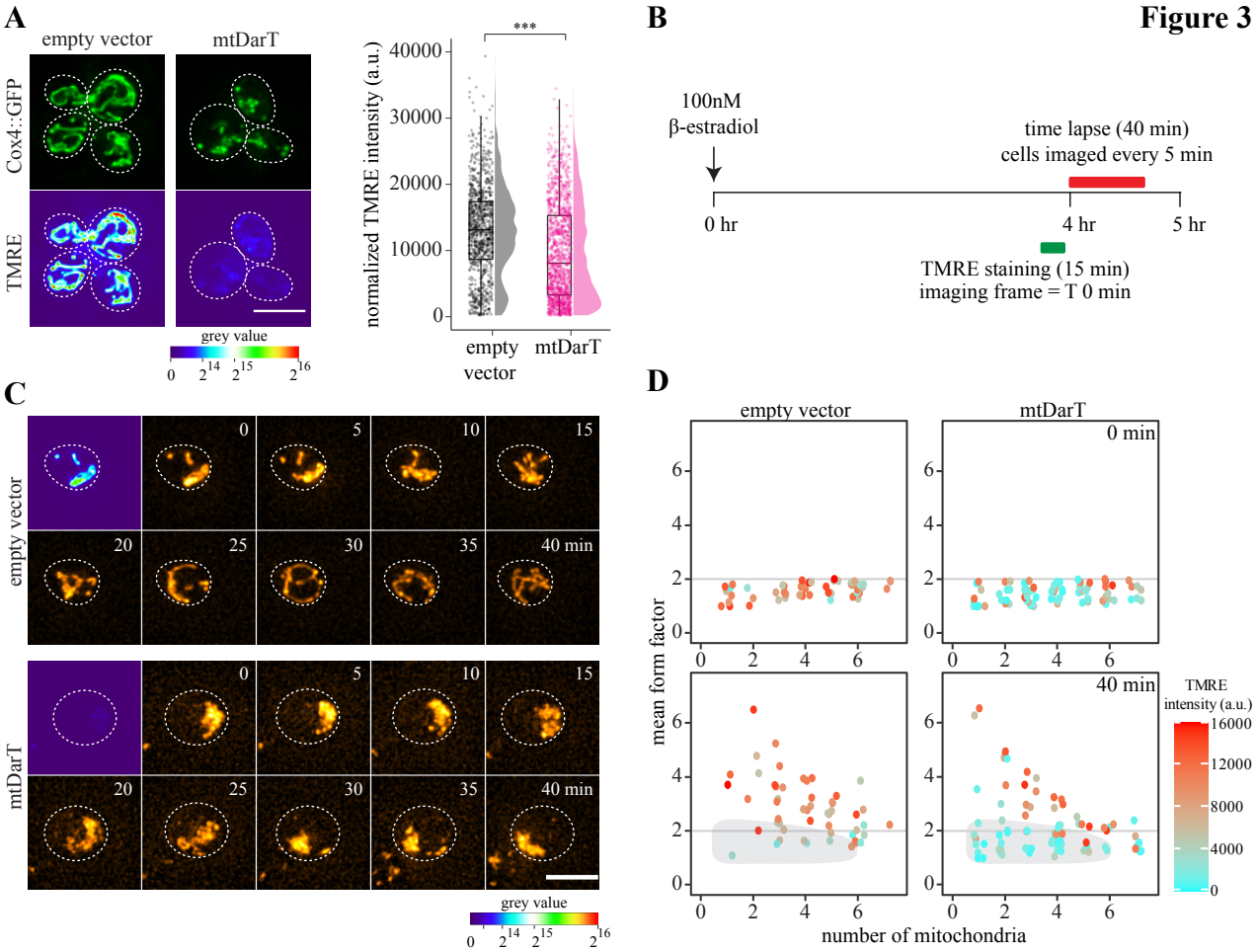
A
empty vector
mtDarT
Cox4::GFP
TMRE
grey value
0
2^14
2^15
2^16
normalized TMRE intensity (a.u.)
40000
30000
20000
10000
0
***
empty vector
mtDarT
B
100nM
β-estradiol
time lapse (40 min)
cells imaged every 5 min
0 hr
4 hr
5 hr
TMRE staining (15 min)
imaging frame = T 0 min
C
empty vector
mtDarT
0
5
10
15
20
25
30
35
40 min
grey value
D
empty vector
mtDarT
0 min
40 min
mean form factor
number of mitochondria
TMRE
intensity (a.u.)
16000
12000
8000
4000
0

Figure 4

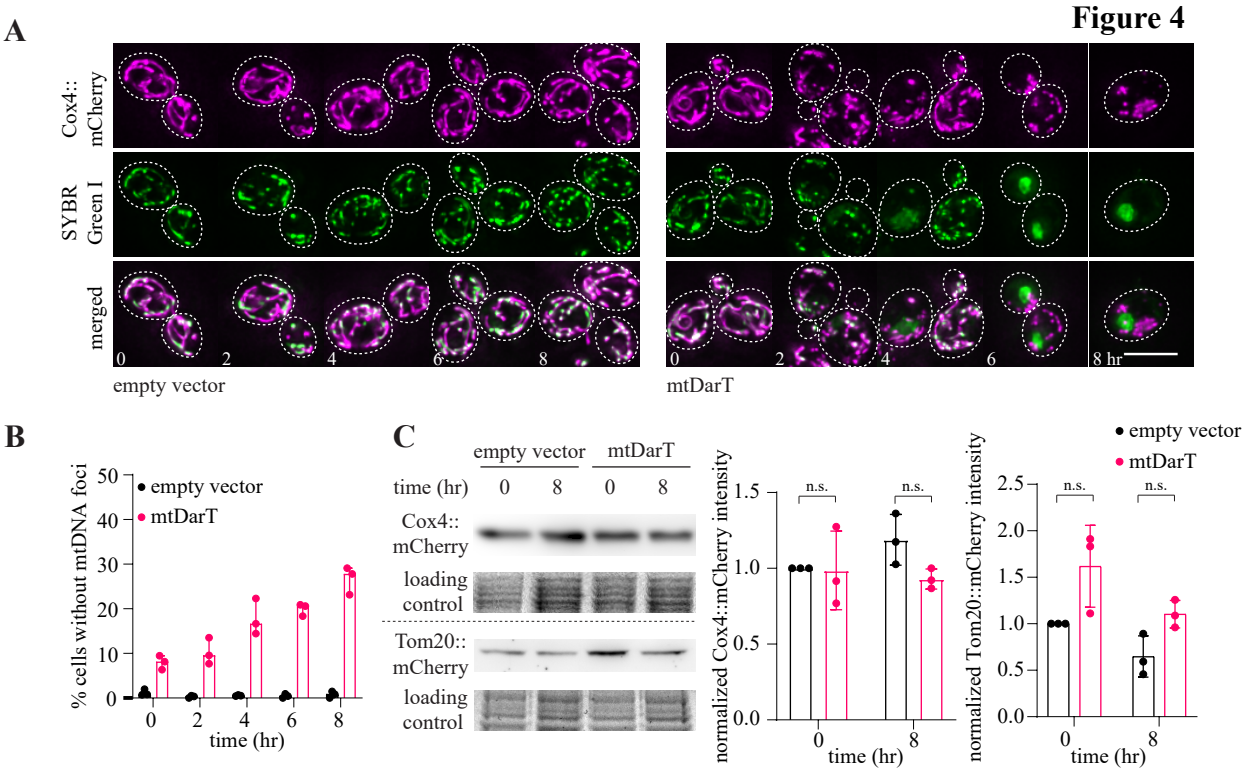
A
Cox4:: mCherry
SYBR Green I
merged
0
2
4
6
8
8 hr
empty vector
mtDarT
B
% cells without mtDNA foci
empty vector
mtDarT
time (hr)
C
empty vector
mtDarT
time (hr)
Cox4:: mCherry
loading control
Tom20:: mCherry
loading control
normalized Cox4::mCherry intensity
normalized Tom20::mCherry intensity
n.s.

Figure 5

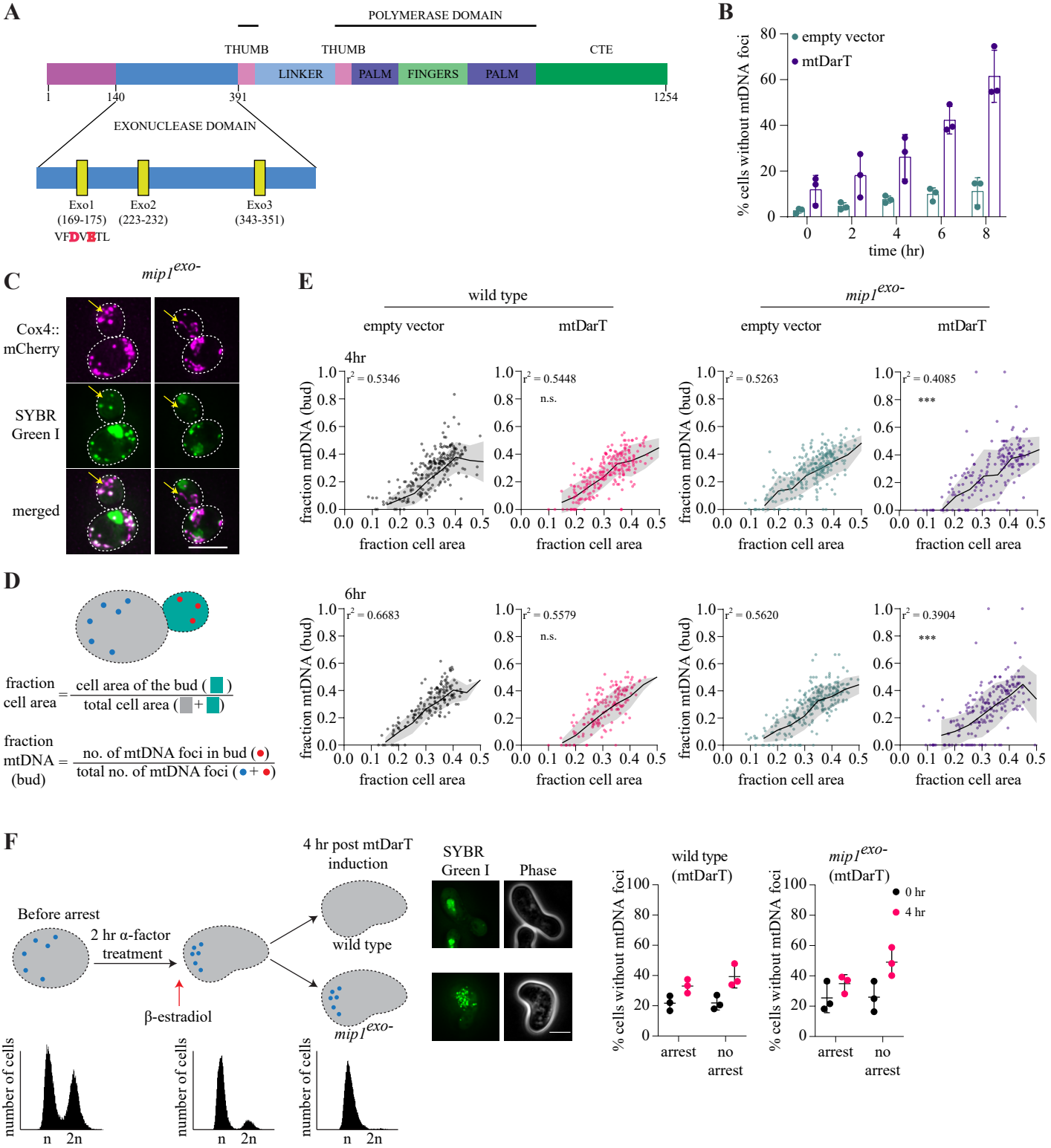
A
POLYMERASE DOMAIN
THUMB
THUMB
CTE
LINKER
PALM
FINGERS
PALM
1
140
391
1254
EXONUCLEASE DOMAIN
Exo1 (169-175)
Exo2 (223-232)
Exo3 (343-351)
VFDVETL
B
empty vector
mtDarT
% cells without mtDNA foci
time (hr)
C
mip1exo-
Cox4:: mCherry
SYBR Green I
merged
D
fraction cell area = cell area of the bud / total cell area
fraction mtDNA (bud) = no. of mtDNA foci in bud / total no. of mtDNA foci
E
wild type
mip1exo-
empty vector
mtDarT
4hr
6hr
fraction mtDNA (bud)
fraction cell area
r2 = 0.5346
r2 = 0.5448
n.s.
r2 = 0.5263
r2 = 0.4085
***
r2 = 0.6683
r2 = 0.5579
n.s.
r2 = 0.5620
r2 = 0.3904
***
F
Before arrest
2 hr α-factor treatment
β-estradiol
4 hr post mtDarT induction
wild type
mip1exo-
number of cells
n
2n
SYBR Green I
Phase
wild type (mtDarT)
mip1exo- (mtDarT)
% cells without mtDNA foci
0 hr
4 hr
arrest
no arrest

Supplementary information

Dynamic reorganization and selective segregation of mitochondria under DarT-mediated mtDNA damage

Nitish Dua, Akshaya Seshadri and Anjana Badrinarayanan*

National Centre for Biological Sciences - Tata Institute of Fundamental Research, Bellary Road, Bangalore 560065, Karnataka, India, Phone: 91 80 23666547

*Correspondence to: anjana@ncbs.res.in

Supplementary figure legends

Figure S1: System to induce mitochondria-specific DNA damage. (A) Schematic of β-estradiol inducible system. Transcription factor GAL4-HBD-VP16 is constitutively expressed under a pACT1 promoter, and is activated on binding of β-estradiol. The activated transcription factor binds to pGAL1 and initiates transcription of gene under this promoter. (B) Western blots of FLAG-tagged mtDarT/TE160A after 4 and 8 hr of induction with 100nM β-estradiol. (C) Representative cells expressing mt-mNeongreen and Cox4::mCherry (top panel), and cell expressing mt-mNeongreen stained with TMRE (bottom panel). (D) Representative cells expressing Lcd1::mNeongreen post 6 hr of mtDarT induction or 2hr post Hydroxyurea (100mM) treatment. Percentage cells with or without Lcd1::mNeongreen foci is plotted. N>400 cells pooled from 2 biological replicates. (Scale bars-5µm, white dotted lines mark cell outlines, in all figures)

Figure S2: mtDNA damage impacts mitochondrial organization and dynamics. (A) Percentage of cells in each category in control (empty vector) or mtDarT cells at t=0hr (mean±SD from three biological replicates, n>150 in each replicate). (B) Schematic showing experimental design for time lapse experiments. (C) Montage of single cells expressing Cox4::mCherry tracked over time (mean form factor <2 at the beginning of the time lapse), imaged for 40 min after 4 hr of induction. T0 refers to the frame at the start of the imaging (after the period of pre-induction) here and in Fig. S2D. (D) Density plots with mean form factor and number of mitochondria over time, plotted for cells starting with MFF>2 at the beginning of time lapse; n=362 for empty vector, n=347 for mtDarT from 3 biological replicates. (E) Dnm1::HA and Fzo1::HA western blot with quantification from 3 biological replicates, normalized to empty vector at t=0; Error bars: SD. (F) Representative images of cells expressing Mdm34::mNeongreen and Cox4::mCherry after 8 hr of induction. Number of Mdm34 foci per cell are plotted from 3 biological replicates; n>680. (G) Cell survival on plates containing either dextrose or glycerol as a carbon source, to ensure C-terminal tagging of Fzo1 does not affect cell growth. Statistical significance in E was calculated using unpaired Student's t-test. (*** p<0.0001, ** p<0.005, * p< 0.05, n.s.- not significant, in all cases).

Figure S3: mtDNA damage impacts mitochondrial organization and dynamics. (A) Cell area plotted as violin plots for all the cells in Fig 2 and S2D at t=0 min. (B) Density plots with Mean form factor and number of mitochondria over time, plotted for cells in Fig 2F, classified based

on presence or absence of buds. T0 refers to the frame at the start of the imaging (after the period of pre-induction)

Figure S4: mtDNA damage results in mitochondrial dysfunction. (A) Representative images of cells expressing Cox4::GFP stained with TMRE after treatment with FCCP (2 µM) for 20 min or Oligomycin (0.5 µg/ml) for 4 hr (left panel) (Cox4::GFP: green). Total TMRE intensity normalized to cell area is plotted; n>650 from 3 biological replicates for FCCP and Oligomycin and 2 biological replicates for empty vector (right panel). (B) Oxygen consumption rate (OCR) estimated using Seahorse assay post 4hr of induction. Mean and SD plotted from technical replicates. (C) Cox2 western blot with quantification from 3 biological replicates, normalized to empty vector at t=0; Error bars: SD. (D) Representative images of cells expressing COX4::GFP stained with TMRE after 4 hr of induction with 100nM β-estradiol. Examples show cells from three different morphological categories for both empty vector and mtDarT (top panel). Total TMRE intensity normalized to cell area is plotted for cells with three mitochondrial morphologies, after 4 hr of induction (for empty vector, n=215 for tubular, n=35 for fragmented, n=30 aggregate; for mtDarT, n=258 for tubular, n=79 for fragmented, n=118 for aggregate). Statistical significance in A, D was calculated using Mann-Whitney U test.

Figure S5: Changes in mitochondrial morphology accompany loss of mtDNA but not mitochondria. (A) Number of mtDNA foci per cell after 8 hr of induction is plotted; n>930 from 3 biological replicates. (B) Representative cells imaged with Structured Illumination Microscopy, along with segmentation output after Mitograph analysis (left panel). Mitochondrial volume was analysed via estimation of number of voxels detected using Mitograph, each data point represents one cell; n=12 for empty vector and n=24 for mtDarT. (C) Representative images of cells expressing GFP::Atg8 under the endogenous *ATG8* promoter treated with Rapamycin (20nM) for 4 hr and cells transformed with empty vector or mtDarT after 8 hs of induction with 100nM β-estradiol (left panel). Frequency distribution of number of GFP::Atg8 localization (right panel). (D) Representative cells showing GFP::Atg8 localizations associated or non-associated with mitochondria. Percentage localizations associated with mitochondria is plotted post 8 hr of induction, or 4 hr of rapamycin (20nM) treatment. Data is pooled from 2 biological replicates. N>90 localizations. (E) Vacuolar intensity of Idh1::GFP normalized to total cell intensity after 4 hr of induction with 100nM β-

estradiol; n>830 from 2 biological replicates (left panel), with representative images of cells expressing Idh1::GFP and Vph1::mCherry (right panel). Statistical significance in A,B,E was calculated using Mann-Whitney U test.

Figure S6: Exonuclease activity of the mtDNA polymerase, Mip1, is essential for mtDNA maintenance. (A) Density plots with mean form factor and number of mitochondria over time for *mip1*$^{exo-}$ cells; n>710 in each plot, from 3 biological replicates. (B) Total TMRE intensity normalized to cell area for *mip1*$^{exo-}$ cells is plotted; n>1350 from 3 biological replicates. (C) Schematic summarizing key observations of this study. mtDNA damage triggers mitochondrial dysfunction and associated changes in mitochondrial organization. Exonuclease function of replicative polymerase, Mip1, is required to prevent rapid loss of mtDNA under damage. For details, see discussion. Statistical significance in B was calculated using Mann-Whitney U test.

Supplementary Table S1: Strains used in present study

Strain #	Strain name	Genotype	Source	Strain construction
NABC567	CEN.PK	*Mat a*	(van Dijken et al., 2000)	NA
NABC568	CEN.PK	*Mat α*	(van Dijken et al., 2000)	NA
NABC569	*COX4-mCherry*	CEN.PK a *COX4-mCherry-Hyg*	This study	mCherry-Hyg casette was amplified from NABC549 using oligos 14,15
NABC570	*COX4-GFP*	CEN.PK a *COX4-GFP-KanMX6*	This study	GFP-KanMX casette was amplified from NABC548 using oligos 14,15
NABC571	*DNM1-HA*	CEN.PK a *DNM1-HA-KanMX6*	This study	HA-KanMX casette was amplified from NABC550 using oligos 17,18
NABC572	*mip1Δ*	CEN.PK a *mip1Δ::KanMX6*	This study	KanMX casette was amplified from NABC551 using oligos 26,27
NABC573	*mip1^{exo-}*	CEN.PK a *mip1Δ::mip1^{D171A,E173A}-Hyg*	This study	Oligos 22,23,24,25 used to amplify full length gene in two fragments, to do Gibson assembly with a Hyg casette amplified from NABC552.
NABC574	*TOM20-mCherry*	CEN.PK a *TOM20-mCherry-KanMX6*	SL lab stock	NA
NABC575	*MDM34-mNeongreen COX4-mCherry*	CEN.PK a *MDM34-mNeongreen-KanMX6 COX4-mCherry-Hyg*	This study	mNeongreen-KanMX cassette was amplified from NABC553 using oligos 20,21. The fragment was transformed in NABC569.
NABC576	*Su9-mNeongreen*	CEN.PK a *HO::P_{CYC1}-SU9-mNeongreen-T_{CYC1}-KanMX6*	This study	NABC556 plasmid was transformed in NABC567 to get HO-locus integration
NABC577	*IDH1-GFP VPH1-mCherry*	CEN.PK a *IDH1-GFP-KanMX6 VPH1-mCherry-Hyg*	This study	GFP-KanMX cassette was amplified from NABC548 (oligos 32,33), mCherry-Hyg cassette was amplified from NABC549 (oligos 34,35) and transformed into NABC567.

NABC593	*Fzo1-HA*	CEN.PK α *Fzo1-HA-Hyg*	This study	HA-Hyg casette was amplified from NABC598 using oligos 36,37.
NABC594	*Lcd1-mNeongreen*	CEN.PK a *Lcd1-mNeongreen-KanMX6*	This study	mNeongreen-KanMX cassette was amplified from NABC553 using oligos 38,39.
NABC595	*bar1Δ*	CEN.PK a *bar1Δ::KanMX6*	SL lab stock	NA
NABC596	*bar1Δ mip1exo-*	CEN.PK a *bar1Δ::KanMX6 mip1Δ::mip1D171A,E173A-Hyg*	This study	NABC595 cells were crossed with NABC597 and sporulated.
NABC597	*mip1exo- α*	CEN.PK α *mip1Δ::mip1^{D171A,E173A}-Hyg*	This study	NABC573 cells were crossed with NABC568 and sporulated.

Supplementary Table S2: Plasmids used in present study

Plasmid #	Plasmid Name	Description	Source	Plasmid construction
NABC548	pFA6a-GFP-KanMX6	Used for C-terminal tagging with GFP and KanMX6 selection marker.	SL lab stock	NA
NABC549	pFA6a-mCherry-Hyg	Used for C-terminal tagging with mCherry and Hygromycin selection marker.	SL lab stock	NA
NABC550	pFA6a-HA-KanMX6	Used for C-terminal tagging with HA and KanMX6 selection marker.	SL lab stock	NA
NABC551	pFA6a-KO-KanMX6	Used for gene knockouts with KanMX6 selection marker.	SL lab stock	NA
NABC552	pFA6a-KO-Hyg	Used for gene knockouts with Hygromycin selection marker.	SL lab stock	NA
NABC553	pFA6a-mNeongreen-KanMX6	Used for C-terminal tagging with mNeongreen and KanMX6 selection marker. Codon optimized mNeongreen was cloned into the pFA6a plasmid background.	This Study	mNeongreen from plasmid NABC554 was cloned with tADH1 into pFA6a background between Pac1 and Bgl2 sites using Gibson cloning with

				oligos 28,29,30,31
NABC554	pMA-Su9-mNeongreen	Codon optimised Su9-mNeongreen sequence.	This Study	(Synthesized by ThermoFisher)
NABC555	p417-CYC	cen/ars plasmid, with weak cyc promoter for low expression of protein	SL lab stock	NA
NABC556	M4297 HO-pCYC1-Su9-mNEONgreen-tCYC1-KanMX6-HO	Used for integration of pCYC1-Su9-mNEONgreen-tCYC1-KanMX6 at HO locus. Plasmid contains overhangs for recombination at the HO locus.	This Study	pCYC1-Su9-mNeongreen-tCYC1 cloned at BamH1 site in NABC 565 using Gibosn cloning with oligos 1,2,3,4
NABC557	pGEV-3XFlag-NAT	*CEN/ARS* Plasmid containing constitutively expressed pGAL4-HBD-VP16 transcription factor under pACT1. Expression of genes cloned under pGAL1 promoter is induced on addition of β-estradiol.	SL lab stock	NA
NABC558	pACDH-DarG	DarG cloned under a Lac promoter (IPTG inducible).	This Study	DarG from NABC560 cloned into NABC566 at Nco1 site using Gibson cloning with oligos 5,6
NABC559	pBAD33-TaqDarT	DarT from *Thermus aquaticus* cloned in the pBAD33 plasmid. Expression is repressed in presence of glucose.	(Jankevicius et al., 2016)	NA
NABC560	pET28a-TaqDarG	DarG from *Thermus aquaticus* cloned in the pET28a plasmid. Expression is repressed in presence of glucose.	(Jankevicius et al., 2016)	NA
NABC561	pGEV-Su9-DarT-3XFlag-NAT	Su9-DarT was cloned at the PacI site downstream of pGAL1 and in frame with the linker-3XFlag sequence.	This Study	DarT from NABC559 cloned with Su9 in NABC557 at PacI site

				using Gibson cloning with oligos 7,10,11,12
NABC562	pGEV-Su9-DarT(E160A)-3XFlag-NAT	Su9-DarT(E160A) was cloned at the PacI site downstream of pGAL1 and in frame with the linker-3XFlag sequence.	This Study	DarT from NABC559 cloned with Su9 in NABC557 at PacI site using Gibson cloning with oligos 7,10,11,12 and oligos 8,9 to introduce mutations
NABC563	GFP-ATG8(416)	N-terminally GFP tagged ATG8 expressed under the control of endogeneous promoter in a pRS416 vector	Addgene (Plasmid #49425) (Guan et al., 2001)	NA
NABC564	p417-GFP-ATG8(416)	GFP-Atg8(416) along with Atg8 promoter cloned between SacI and EcoRI sites	This Study	GFP-Atg8 with endogeneous Atg8 promoter was cloned from NABC563 into NABC555 by restriction digestion and ligation using restriction sites for SacI and EcoRI
NABC565	M4297HO Kan	HO-locus integration plasmid with KanMX selection marker	SL lab stock	NA
NABC566	pACDH	Plasmid with a lac promoter and a p15a ori	SL lab stock	NA
NABC598	pFA6a-HA-Hyg	Used for C-terminal tagging with HA and Hygromycin selection marker.	SL lab stock	NA

Supplementary Table S3: Oligos used in present study

Oligo #	Oligo sequence (5'-3')
Oligo 1	cgcaaacacaaatacacacactaatctagaATGGCTTCTACTAGAGTTTTGGCTTCTAGA TTGGCTTCTCA
Oligo 2	ctgcagcccgggggatccactagttctagaTCAAGAATTAGAAGAAGCAGAACCTGAACC TGCAGCAGA
Oligo 3	TTAAAATGGCGTCGTACGCTGCAGGTCGACGGATCCcatttggcgagcgttggttggtggatcaag
Oligo 4	AACAGATCTGGCGCGCCTTAATTAACCCGGGGATCCgcaaattaaagccttcgagcg tcccaaaaccttctc
Oligo 5	GTTTAACTTTAAGAAGGAGATATACCATGGATGCTGCGTTTCGTTCGCGGTAAC
Oligo 6	TTTGCTGTCCACCAGTCATGCTAGCCATGGTTACGCTTCTTGAGCAACATT TGCCGGC
Oligo 7	GATACTCAAAGATATCCCCGGGTTAATTAAATGGCTTCTACTAGAGTTTT GGCTTCTAG
Oligo 8	CTTTGACCAGAAATGCGGCCTGTTTC
Oligo 9	GAAACAGGCCGCATTTCTGGTCAAAG
Oligo 10	GTCATCGTCATCTTTATAATCGTTAATTAAGAACGTGGCTTCACAGGACGCACTGC
Oligo 11	AACCGGATAAGCCAGACCCTGTTGCGGCAT AGAAGAGTAGGCCCTTTTT TGAAAAGC
Oligo 12	ATGCCGCAACAGGGTCTGGCTTATCC
Oligo 13	GAAAACTGCCCAAAACTTAG
Oligo 14	ACTAAACCCTGTTGGTGTTCCAAATGATGACCACCATCACcggatccccgggttaattaa
Oligo 15	GTAAAAGAGAAACAGAAGGGCAACTTGAATGATAAGATTAgaattcgagctcgtttaaac
Oligo 16	CGGTGATGGAAATATTGAAG
Oligo 17	AGTTTATAAAAAGGCTGCAACCCTTATTAGTAATATTCTGcggatccccgggttaattaa
Oligo 18	TGTTGAAGTAAGATCAAAAATGAGATGAATTATGCAATTAgaattcgagctcgtttaaac
Oligo 19	GATTCAGTCTCGACTTTTCG
Oligo 20	CTGGAAATGGGGCATGGAGGATAGCCCCCCACCATATCATcggatccccgggttaattaa
Oligo 21	TATTTGTGTAGTTATGTACTTAGATATGTAACTTAATTTAgaattcgagctcgtttaaac
Oligo 22	TATGTAGTTGTTGAGCAACGAGGGACAAGTATGACGAAATTGATGGTTAG ATCTGAATGCATGCTG
Oligo 23	CTGGTGGTGTTTGCTGTAGCAACACTCTATAAC
Oligo 24	CGTTATAGAGTGTTGCTACAGCAAACACCACCAG
Oligo 25	CTAGTACTCTCTAGAAATAGTAATGTCCCTTTCCAG
Oligo 26	GGGATTATATGTAGTTGTTGAGCAACGAGGGACAAGTATGcggatccccgggttaattaa
Oligo 27	ATATAAATACAAATGCGAAAGCTAATGCAGATTTTGCCTAgaattcgagctcgtttaaac
Oligo 28	TGCAGGTCGAcggatccccgggttaattaaCATGGCTTCTTTGCCAGCTAC
Oligo 29	aataaaaatcataaatcataagaaattcgcTCAAGAATTAGAAGAAGCAGAACCTGAA
Oligo 30	gcgaatttcttatgatttatgattt
Oligo 31	cggcggggacgaggcaagctaaacagatct
Oligo 32	TGACTTCACGAATGAAATCATCAACAAATTATCTACCATGcggatccccgggttaattaa
Oligo 33	TTAAGTTGCAGAACAAAAAAAAGGGGAATTGTTTTCATTAgaattcgagctcgtttaaac
Oligo 34	GGAAGTCGCTGTTGCTAGTGCAAGCTCTTCCGCTTCAAGCcggatccccgggttaattaa
Oligo 35	ACTTAAATGTTTCGCTTTTTTTAAAAGTCCTCAAAATTTAgaattcgagctcgtttaaac
Oligo 36	TCAAAAATTGATGGTGGAAGAAATAAATTTAGACATCGATcggatccccgggttaattaa

Oligo 37	ATTGATTTGAAAAGACCTCATATATTTACAAGAATATCTAgaattcgagctcgtttaaac
Oligo 38	ACTAGAGGAGGCCGATTCATTATATATCTCAATGGGACTGcggatccccgggttaattaa
Oligo 39	TATAAAGCGTTGACATTTTCCCCTTTTGATTGTTGCCTTAgaattcgagctcgtttaaac

Supplementary references

Guan, J., Stromhaug, P. E., George, M. D., Habibzadegah-Tari, P., Bevan, A., Dunn, W. A., & Klionsky, D. J. (2001). Cvt18/Gsa12 is required for cytoplasm-to-vacuole transport, pexophagy, and autophagy in Saccharomyces cerevisiae and Pichia pastoris. *Molecular Biology of the Cell*, *12*(12), 3821–3838. https://doi.org/10.1091/mbc.12.12.3821

Jankevicius, G., Ariza, A., Ahel, M., & Ahel, I. (2016). The Toxin-Antitoxin System DarTG Catalyzes Reversible ADP-Ribosylation of DNA. *Molecular Cell*, *64*(6), 1109–1116. https://doi.org/10.1016/j.molcel.2016.11.014

van Dijken, J. P., Bauer, J., Brambilla, L., Duboc, P., Francois, J. M., Gancedo, C., Giuseppin, M. L. F., Heijnen, J. J., Hoare, M., Lange, H. C., Madden, E. A., Niederberger, P., Nielsen, J., Parrou, J. L., Petit, T., Porro, D., Reuss, M., van Riel, N., Rizzi, M., … Pronk, J. T. (2000). An interlaboratory comparison of physiological and genetic properties of four Saccharomyces cerevisiae strains. *Enzyme and Microbial Technology*, *26*(9), 706–714. https://doi.org/10.1016/S0141-0229(00)00162-9

Figure S1

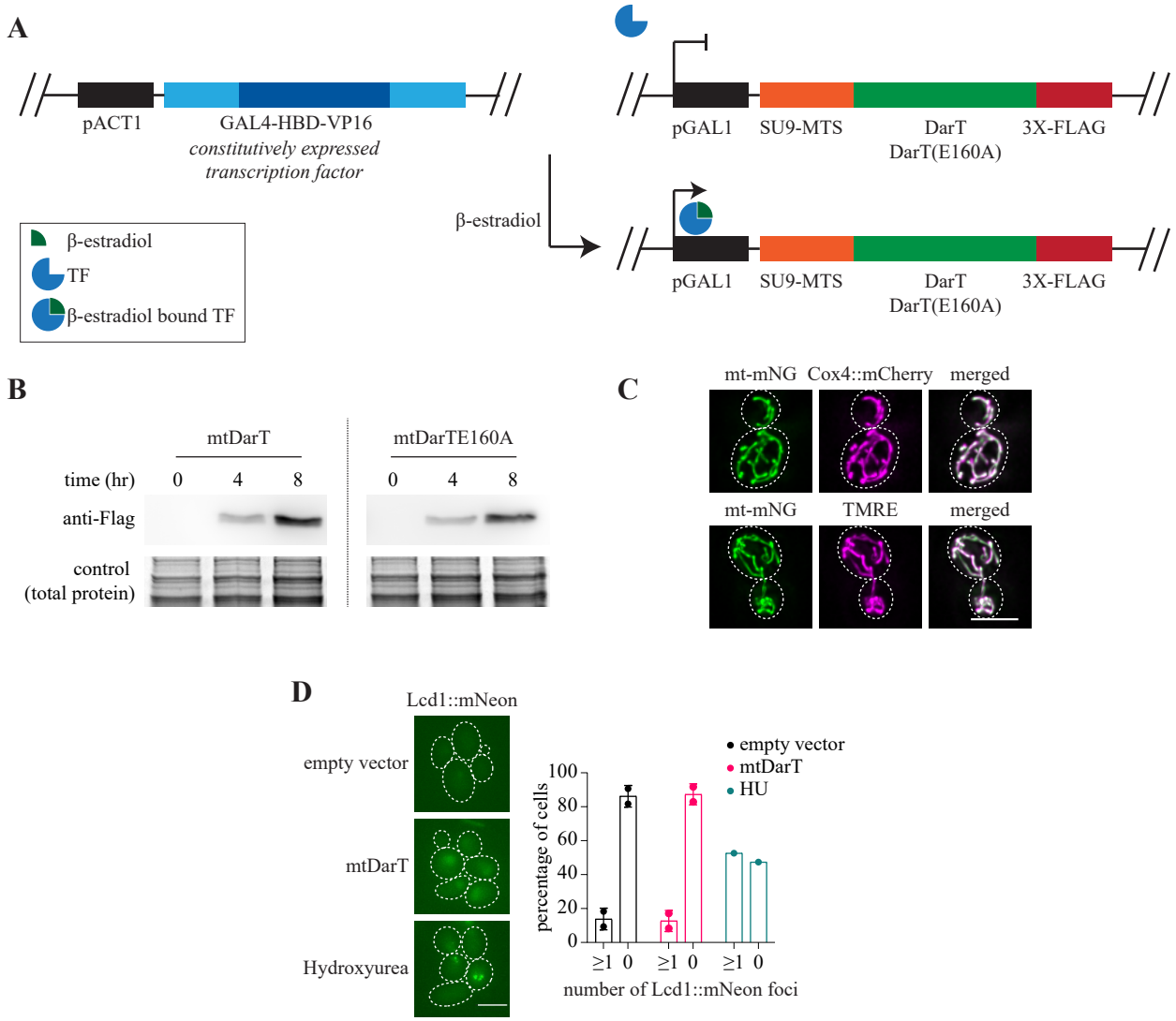
A
pACT1
GAL4-HBD-VP16
constitutively expressed transcription factor
β-estradiol
TF
β-estradiol bound TF
pGAL1
SU9-MTS
DarT
DarT(E160A)
3X-FLAG
β-estradiol
pGAL1
SU9-MTS
DarT
DarT(E160A)
3X-FLAG
B
mtDarT
mtDarTE160A
time (hr)
0
4
8
0
4
8
anti-Flag
control
(total protein)
C
mt-mNG
Cox4::mCherry
merged
mt-mNG
TMRE
merged
D
Lcd1::mNeon
empty vector
mtDarT
Hydroxyurea
empty vector
mtDarT
HU
percentage of cells
100
80
60
40
20
0
≥1
0
≥1
0
≥1
0
number of Lcd1::mNeon foci

Figure S2

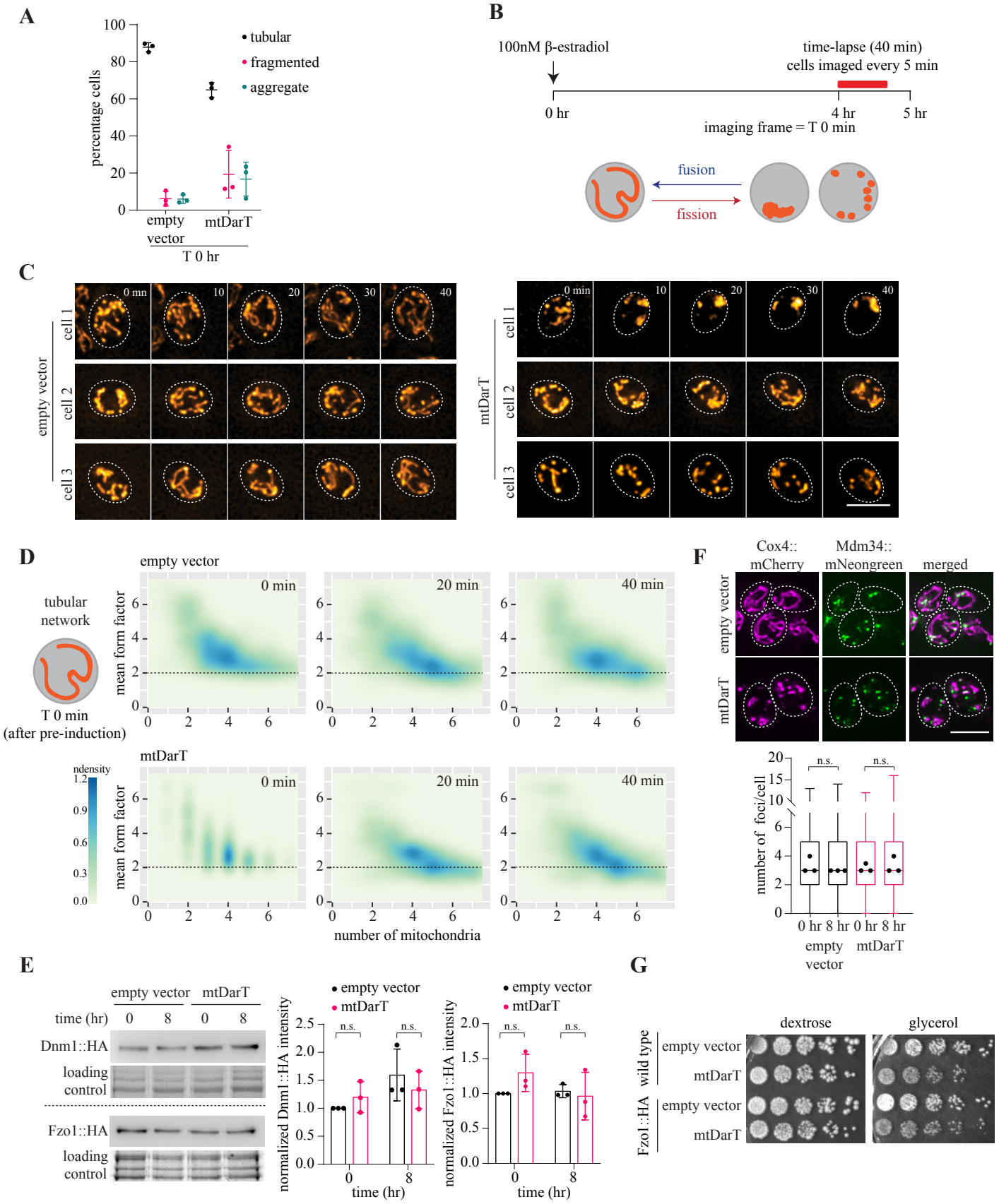
A
percentage cells
tubular
fragmented
aggregate
empty vector
mtDarT
T 0 hr
B
100nM β-estradiol
time-lapse (40 min)
cells imaged every 5 min
0 hr
4 hr
5 hr
imaging frame = T 0 min
fusion
fission
C
empty vector
mtDarT
cell 1
cell 2
cell 3
0 mn
10
20
30
40
D
empty vector
mtDarT
tubular network
T 0 min (after pre-induction)
mean form factor
0 min
20 min
40 min
ndensity
number of mitochondria
E
empty vector
mtDarT
time (hr)
Dnm1::HA
loading control
Fzo1::HA
normalized Dnm1::HA intensity
normalized Fzo1::HA intensity
n.s.
time (hr)
F
Cox4:: mCherry
Mdm34:: mNeongreen
merged
number of foci/cell
0 hr 8 hr 0 hr 8 hr
empty vector
mtDarT
G
dextrose
glycerol
wild type
Fzo1::HA

Figure S3

A

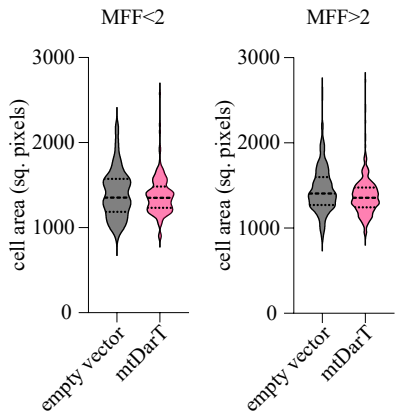
MFF<2
MFF>2
cell area (sq. pixels)
3000
2000
1000
0
empty vector
mtDarT

B

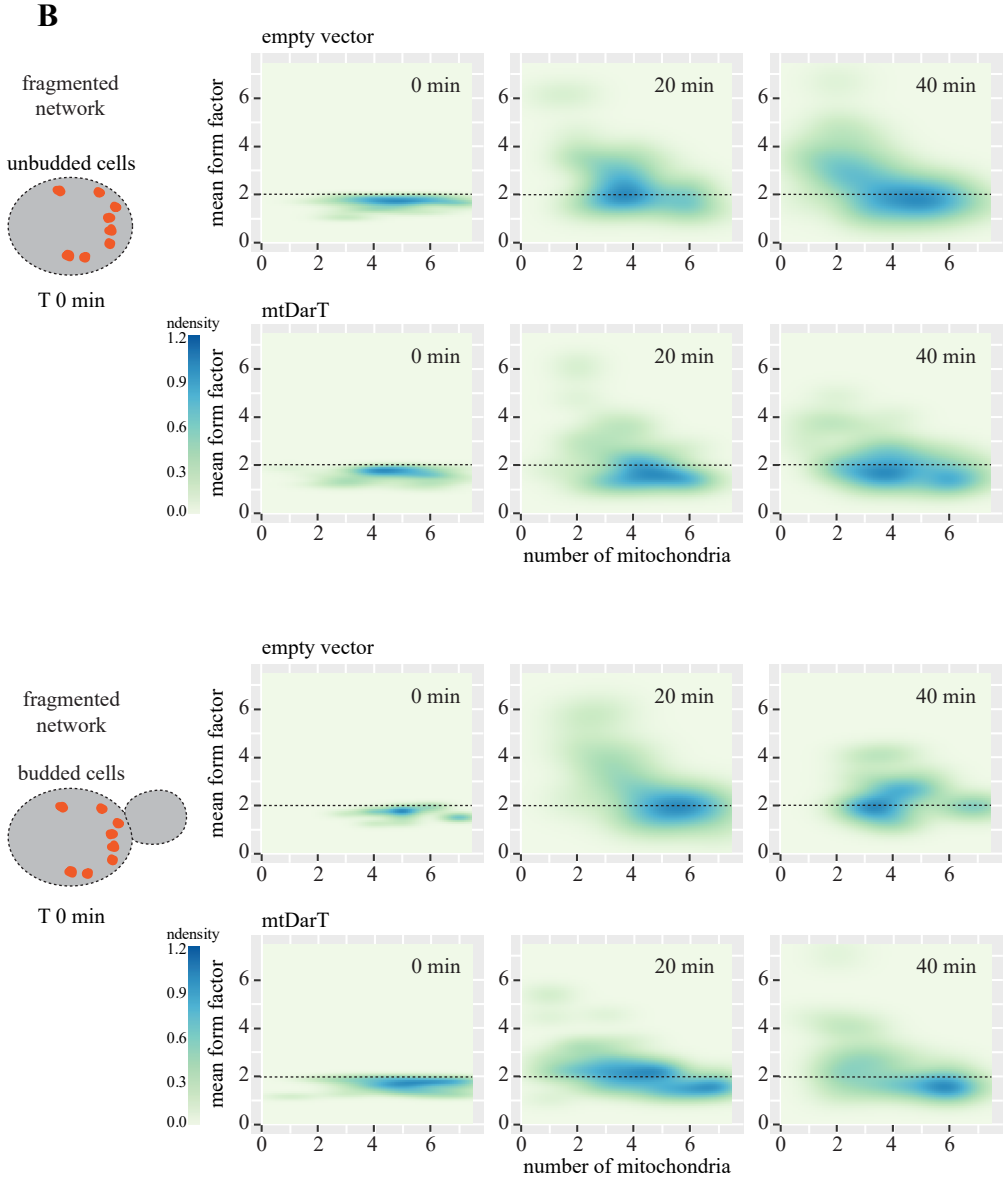
fragmented network
unbudded cells
T 0 min
budded cells
empty vector
mtDarT
0 min
20 min
40 min
mean form factor
number of mitochondria
ndensity
1.2
0.9
0.6
0.3
0.0

Figure S4

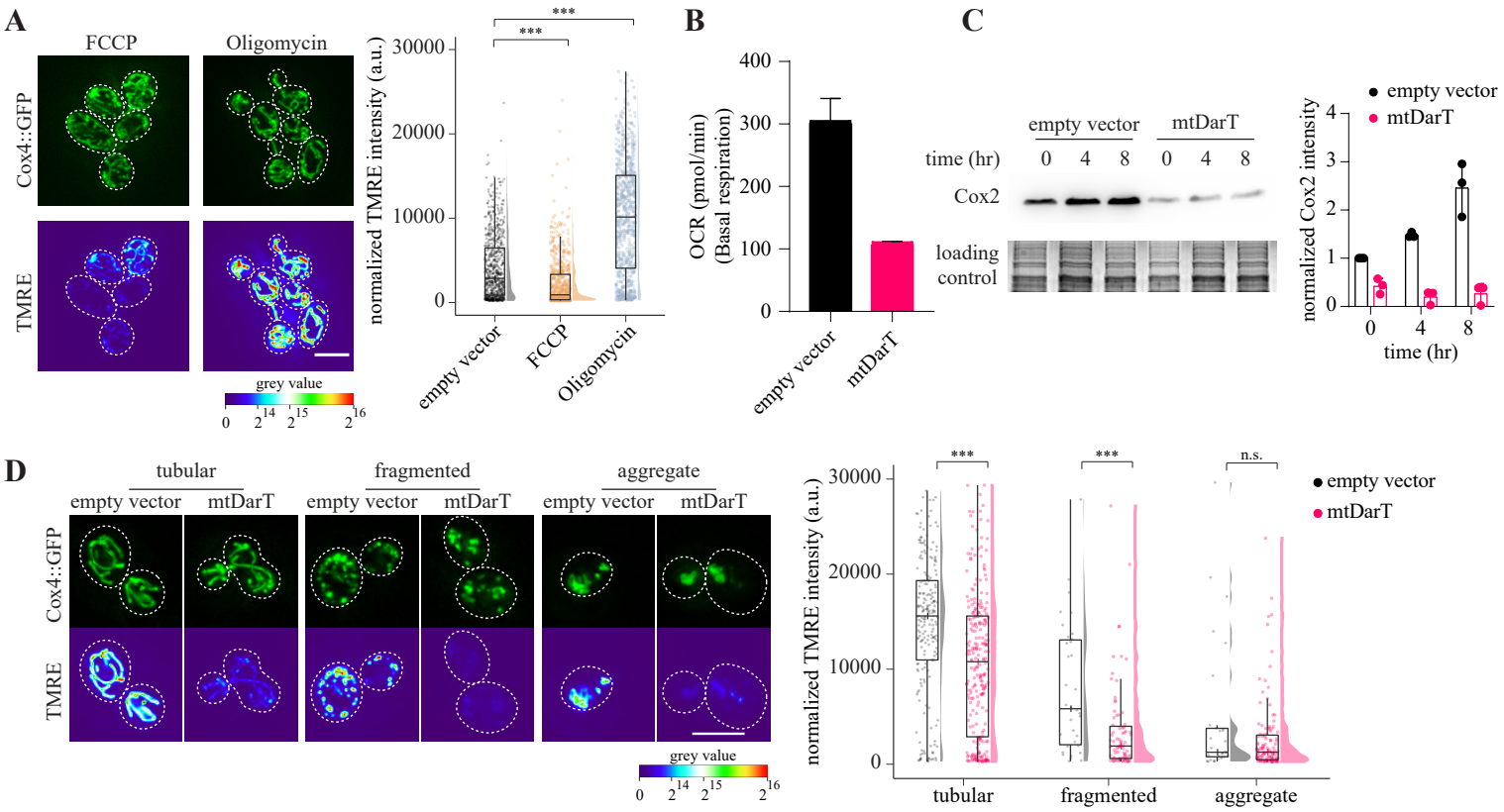
A
FCCP
Oligomycin
Cox4::GFP
TMRE
grey value
normalized TMRE intensity (a.u.)
empty vector
FCCP
Oligomycin
B
OCR (pmol/min)
(Basal respiration)
empty vector
mtDarT
C
empty vector
mtDarT
time (hr)
Cox2
loading control
normalized Cox2 intensity
time (hr)
D
tubular
fragmented
aggregate
empty vector
mtDarT
Cox4::GFP
TMRE
grey value
normalized TMRE intensity (a.u.)
n.s.
tubular
fragmented
aggregate

Figure S5

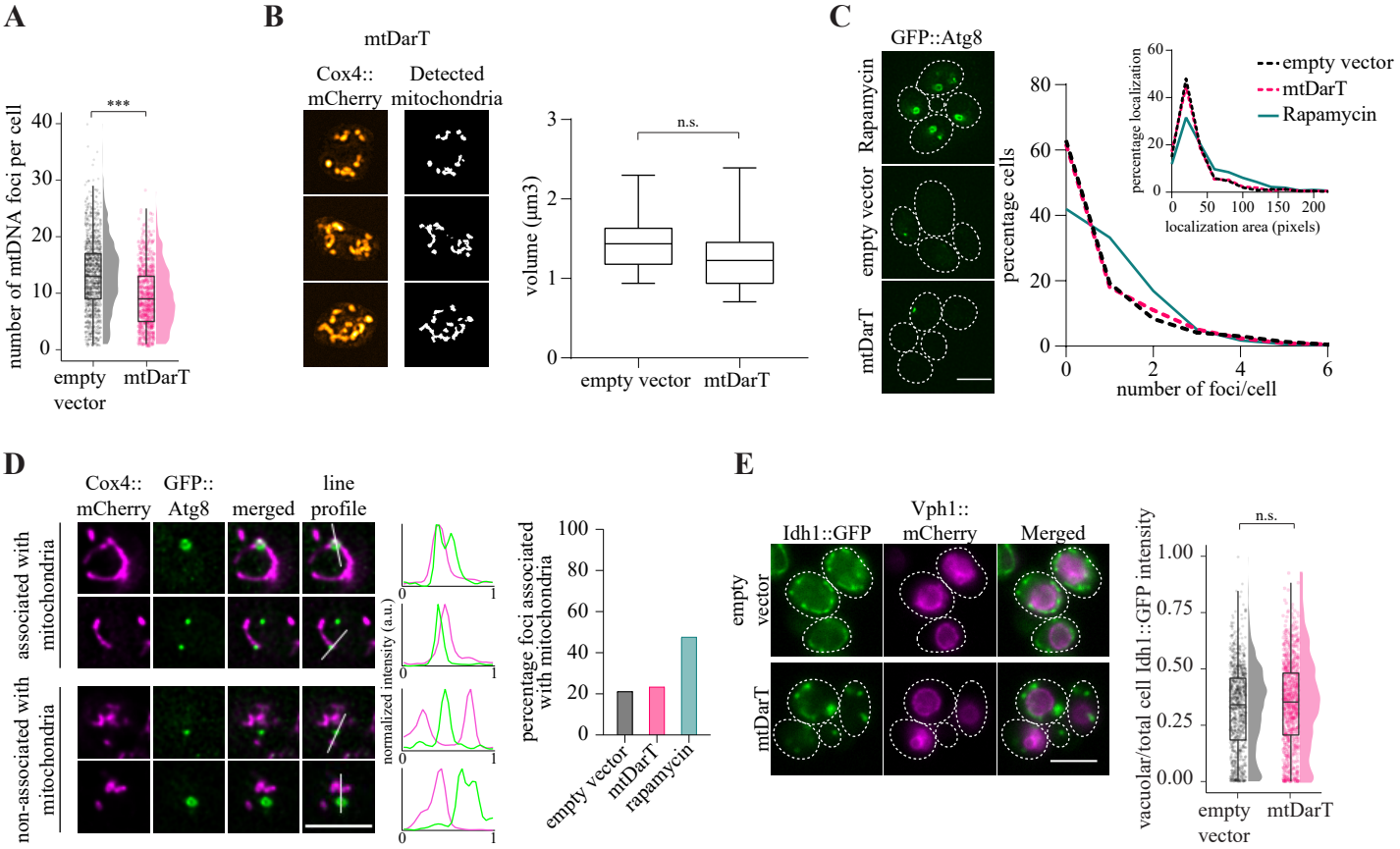
A
number of mtDNA foci per cell
***
empty vector
mtDarT
B
mtDarT
Cox4:: mCherry
Detected mitochondria
volume (µm3)
n.s.
empty vector
mtDarT
C
GFP::Atg8
Rapamycin
empty vector
mtDarT
percentage cells
number of foci/cell
percentage localization
localization area (pixels)
empty vector
mtDarT
Rapamycin
D
Cox4:: mCherry
GFP:: Atg8
merged
line profile
associated with mitochondria
non-associated with mitochondria
normalized intensity (a.u.)
percentage foci associated with mitochondria
empty vector
mtDarT
rapamycin
E
Idh1::GFP
Vph1:: mCherry
Merged
empty vector
mtDarT
vacuolar/total cell Idh1::GFP intensity
n.s.
empty vector
mtDarT

Figure S6

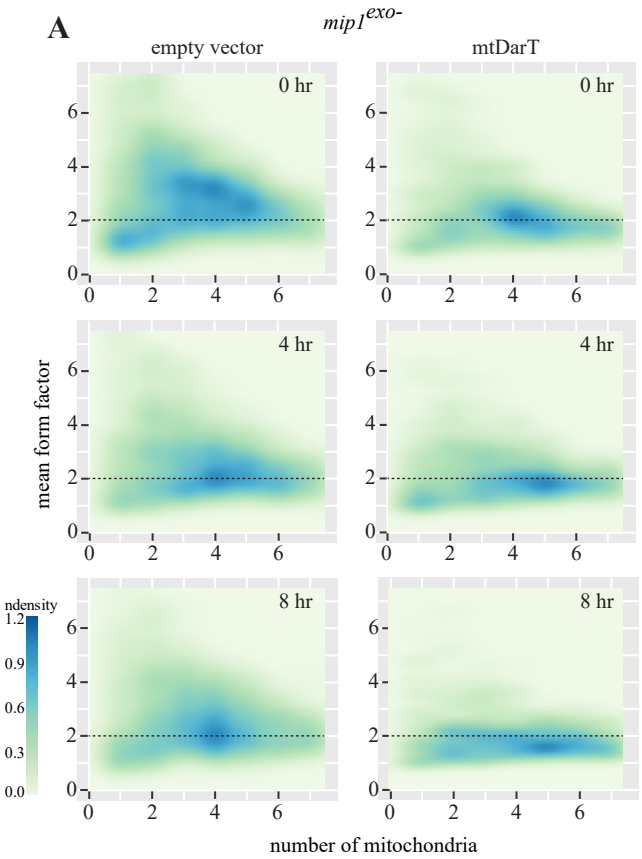
A
mip1exo-
empty vector
mtDarT
0 hr
4 hr
8 hr
mean form factor
ndensity
1.2
0.9
0.6
0.3
0.0
number of mitochondria

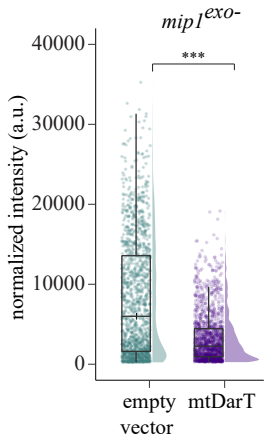
B
mip1exo-
***
normalized intensity (a.u.)
40000
30000
20000
10000
0
empty vector
mtDarT

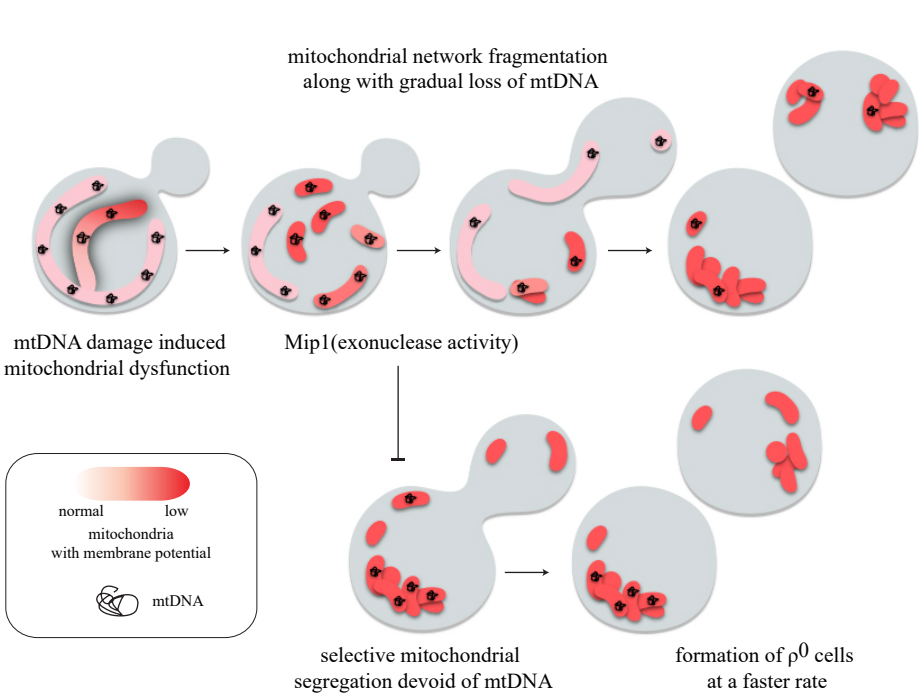
C
mitochondrial network fragmentation
along with gradual loss of mtDNA
mtDNA damage induced
mitochondrial dysfunction
Mip1(exonuclease activity)
normal
low
mitochondria
with membrane potential
mtDNA
selective mitochondrial
segregation devoid of mtDNA
formation of ρ0 cells
at a faster rate